the FEBS Journal

Investigation of the interaction between the atypical agonist c[YpwFG] and MOR

Luca Gentilucci[1], Federico Squassabia[1], Rossella Demarco[1], Roberto Artali[2], Giuliana Cardillo[1], Alessandra Tolomelli[1], Santi Spampinato[3] and Andrea Bedini[3]

1 Dipartimento di Chimica 'G. Ciamician', Università degli Studi di Bologna, Italy
2 Istituto di Chimica Farmaceutica e Tossicologica 'P. Pratesi', Università di Milano, Italy
3 Dipartimento di Farmacologia, Università degli Studi di Bologna, Italy

Keywords
atypical agonist; cyclopentapeptide; induced fit; molecular docking; opioid receptor

Correspondence
L. Gentilucci, Dipartimento di Chimica 'G. Ciamician', Università degli Studi di Bologna, via Selmi 2, 40126-Bologna, Italy
Fax: +39 051 2099456
Tel: +39 051 2099462
E-mail: luca.gentilucci@unibo.it

(Received 8 January 2008, revised 22 February 2008, accepted 6 March 2008)

doi:10.1111/j.1742-4658.2008.06386.x

Endogenous and exogenous opiates are currently considered the drugs of choice for treating different kinds of pain. However, their prolonged use produces several adverse symptoms, and in addition, many forms of pain are resistant to any kind of therapy. Therefore, the discovery of compounds active towards μ-opioid receptors (MORs) by alternative pharmacological mechanisms could be of value for developing novel classes of analgesics. There is evidence that some unusual molecules can bind opioid receptors, albeit lacking some of the typical opioid pharmacophoric features. In particular, the recent discovery of a few compounds that showed agonist behavior even in the absence of the primary pharmacophore, namely a protonable amine, led to a rediscussion of the importance of ionic interactions in stabilizing the ligand–receptor complex and in activating signal transduction. Very recently, we synthesized a library of cyclic analogs of the endogenous, MOR-selective agonist endomorphin-1 (YPWF-NH_2), containing a Gly5 bridge between Tyr1 and Phe4. The cyclopeptide c[YpwFG] showed good affinity and agonist behavior. This atypical MOR agonist does not have the protonable Tyr amine. In order to gain more information about plausible mechanisms of interaction between c[YpwFG] and the opioid receptor, we synthesized a selected set of derivatives containing different bridges between Tyr1 and Phe4, and tested their affinities towards μ-opioid receptors. We performed conformational analysis of the cyclopeptides by NMR spectroscopy and molecular dynamics, and investigated plausible, unprecedented modes of interaction with the MOR by molecular docking. The successive quantum mechanics/molecular mechanics investigation of the complexes obtained by the molecular docking procedure furnished a more detailed description of the binding mode and the electronic properties of the ligands. The comparison with the binding mode of the potent agonist JOM-6 seems to indicate that the cyclic endomorphin-1 analogs interact with the receptor by way of an alternative mechanism, still maintaining the ability to activate the receptor.

In recent years, various research groups have described opioid receptor (OR)-active molecules lacking some crucial pharmacological requisites. In particular, several papers have stressed the role of Tyr1 in the interaction of native or synthetic opioid peptides with μ-opioid receptors (MORs). In certain cases, the

Abbreviations
Aib, α-aminoisobutyric acid; CPP, cyclopentapeptide; DAMGO, H-Tyr-D-Ala-Gly-*N*-MePhe-glyol; DOR, δ-opioid receptor; DPPA, diphenylphosphorylazide; EL, extracellular loop; EM-1, endomorphin-1; KOR, κ-opioid receptor; MD, molecular dynamics; MM, molecular mechanics; MOR, μ-opioid receptor; QM, quantum mechanics; TMH, transmembrane helix; VT, variable temperature.

modification of the phenolic OH group had no consequences for the ability to bind the receptor. Indeed, the transposition [1,2], removal [3,4], duplication [5] or substitution with a surrogate [6] of Tyr1 gave analogs that showed comparable binding affinities and potencies to those of the parent peptides.

A more relevant modification is the removal or derivatization of the positively charged N-terminal amino group. In general, these modifications are responsible for transforming agonists into antagonists, confirming the fundamental role of the amino group in receptor activation. Noteworthy examples are the somewhat δ-opioid receptor (DOR)-selective casomorphin derivatives, in which the terminal amino group is eliminated or formylated [7], the carbamate-peptide $PhCH_2OC(O)$–Pro–Trp–$PheNH_2$, which showed nanomolar affinity for MORs [8], the potent enkephalin-derived DOR antagonist containing a deaminated Tyr [9], the enkephalin and κ-opioid receptor (KOR)-selective DynA analogs obtained by replacement of Tyr1 with 3-(2′,6′-dimethyl-4′-hydroxyphenyl)propanoic acid and (2*S*)-2-methyl-3-(2′,6′-dimethyl-4′-hydroxyphenyl)-propionic acid (Mdp) [10], and finally the cyclic DynA analog lacking the basic N-terminus, which showed good KOR affinity [11].

In contrast, a few compounds lacking the amino group have demonstrated an agonist nature: the MOR-selective bicyclic compound **1**, designed to mimic enkephalin or endomorphin β-turn models, the κ-selective neoclerodane diterpene salvinorin A (compound **2**), and the cyclic endomorphin-1 (EM-1) analog active towards MOR *c*[YpwFG] (compound **3**) (Fig. 1).

The highly constrained 6,6-bicyclic compound **1**, which has no N-terminal amino group, showed an initial level of analgesic activity similar to that of morphine, but with a shorter *in vivo* half-life [12]. On the basis of 2D-NMR analysis and molecular mechanics (MM) computations, the authors noticed a certain superimposition of the structure of compound **1** with a *trans*-EM-1 type III β-turn-like structure. According to this partial superimposition and the MOR selectivity profile, they implicitly suggested that the interaction of compound **1** with the receptor could mimic that of EM-1 or enkephalins, even in the absence of a ionic interaction.

Salvinorin A (compound **2**), a naturally occurring hallucinogen isolated from *Salvia divinorum* [13], is a unique, non-nitrogen-containing selective KOR agonist. An earlier docking analysis, based in turn on models originally developed for non-opioid KOR agonists such as U69593 [14], led to a preliminary model. However, by using an improved model of the receptor, and screening of salvinorin derivatives [15], the same authors substantially modified the original model [16]. More recently, acquired structure–function data of salvinorin analogs [17,18] led to the proposal of a third different model [19].

The cyclopeptide compound **3**, *c*[YpwFG], showed good MOR affinity (Table 1), and agonist behavior (forskolin-stimulated cAMP production inhibition test) [20]. Cyclic peptides have been widely used as conformationally restricted frameworks [21], useful for arranging the pharmacophores in different reciprocal orientations, and in particular, cyclic pentapeptides containing one or two D-amino acids have been successfully utilized as β-turn or γ-turn models [22–27]. The hypothesis that EM-1 derivatives could adopt at the receptor a folded structure stabilized by some kind of γ-turn or β-turn has been stressed in recent papers [8,28,29].

For the atypical structure and the highly lipophilic character, we planned further studies to provide insights into how *c*[YpwFG] might interact with the receptor. We synthesized and tested a selected mini-library of new cyclopeptides derived from compound **3**, and we performed a computational investigation intended to investigate the possible orientations of the biologically active cyclopeptides when docked into the binding site defined by the MOR model. We first

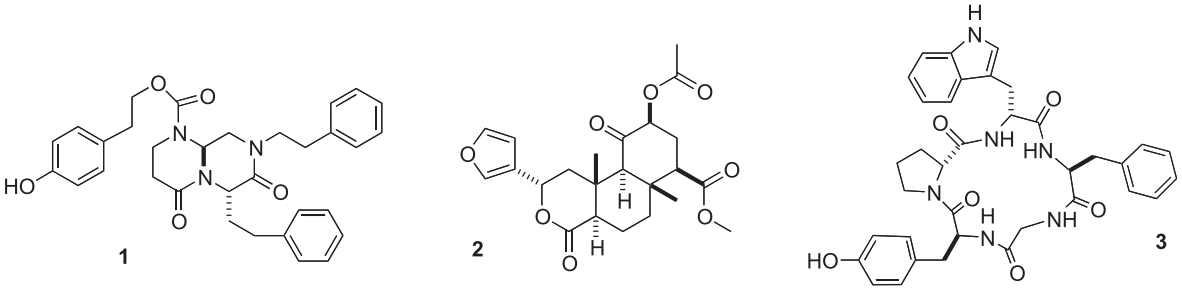

Fig. 1. Examples of opioid agonists lacking a protonable amino group.

Table 1. Synthesis, analytical characterization and receptor affinities (means ± SE of three experiments) of DAMGO and compounds **3**–**8**.

Compound	Sequence	Yield (%)[a]	Purity (%)	MS/calculated [*M* + 1]	K_i (M)	IC_{50} (M)
DAMGO	YaG-*N*MeF-Glyol	–	–	–	$1.6 \pm 0.3 \times 10^{-9}$	$9.9 \pm 0.6 \times 10^{-9}$
3	*c*[YpwFG]	62	96	651.2/651.1	$3.4 \pm 0.7 \times 10^{-8}$	$4.4 \pm 0.6 \times 10^{-8}$
4	*c*[YpwF-βAla]	58	93	665.3/665.3	$6.1 \pm 0.5 \times 10^{-6}$	$1.6 \pm 0.2 \times 10^{-5}$
5	*c*[YpwF-GABA]	64	93	679.5/679.3	$3.2 \pm 0.4 \times 10^{-6}$	$8.4 \pm 0.8 \times 10^{-6}$
6	*c*[YpwF-Aib]	55	95	679.2/679.3	$2.9 \pm 0.3 \times 10^{-6}$	$7.6 \pm 0.7 \times 10^{-6}$
7	*c*[YpwFp]	53	96	691.6/691.3	$3.2 \pm 0.2 \times 10^{-5}$	$8.3 \pm 0.9 \times 10^{-5}$
8	*c*[YpwFP]	59	95	691.5/691.3	$7.2 \pm 0.5 \times 10^{-7}$	$9.0 \pm 0.4 \times 10^{-7}$

[a] Yield of the cyclization step after purification.

explored the possible binding positions and binding modes of the ligand within the rigid receptor environment, and the solutions obtained from this docking study were subsequently optimized by means of the combined quantum mechanics QM/MM approach, using a flexible receptor environment that allows for simulation of the receptor adaptation upon ligand binding (induced fit). The conformations adopted in dimethylsulfoxide were used as starting structures for docking the ligands into the entire channel pore with AUTODOCK [30], without prior specification of the binding site, by using the so-called 'blind docking' approach, a technique introduced for the detection of possible binding sites and modes of binding of peptide ligands by searching the entire surface of protein targets [31,32]. The main potential orientations have been evaluated using the QM/MM optimization of the complexes [33,34], providing a more detailed description of the binding mode and the electronic and steric properties of the c[YpwFG] ligand.

Results

Synthesis and pharmacological characterization of the cyclopeptides c[YpwFXaa]

We synthesized compound **3** as a member of a series of conformationally restricted EM-1 (YPWF-NH_2) derivatives having the first and fourth residues connected by a simple Gly bridge [20]. To define the best spatial disposition of the aromatic side chains for an optimal ligand–receptor interaction, we introduced each 1–4 residue in the D-configuration or L-configuration, generating a library of stereoisomeric, 3D distinct cyclopentaptides. Among the diverse stereoisomers of the library, only compound **3** of sequence c[YpwFG] showed a satisfactory affinity for MORs [20].

Cyclopentapeptides (CPPs) are expected to be relatively conformationally homogeneous. It has been well documented that for most CPPs, the overall conformation depends on the specific sequence of residue chirality, and the nature of the residue should play a minor role [21,26,27]. Therefore, different stereoisomers can reproduce different types of conformational elements of the peptide backbone, as various β-turns, γ-turns, or α-helical structures.

However, despite the constrained structure, these molecules often exhibit a remarkable degree of residual flexibility, especially in the presence of a Gly [21,26]. In principle, the occurrence of a conformational equilibrium between different structures does not prohibit efficient receptor binding, allowing the peptide a certain facility to adapt to the receptor cavity. This conformational freedom could be responsible for the possibility that compound **3** fitted the receptor by adopting alternative backbone conformations.

In order to gain further information about the biologically active structure, we have synthesized a new set of CPPs having the same sequence YpwF as compound **3** and a different amino acid, Xaa, in position 5 in place of Gly, with different structure and length (Fig. 2). We introduced longer, flexible connectors between Tyr1 and Phe4, Xaa5 = β-Ala (compound **4**) and Xaa5 = γ-aminobutyric acid (compound **5**), which in principle should confer the peptide a higher conformational freedom, or conversely, we introduced conformationally restraining residues, Xaa5 = α-aminoisobutyric acid, Aib (compound **6**), Xaa5 = D-Pro (compound **7**), and Xaa5 = L-Pro (compound **8**). In particular, Aib in an oligopeptide predominantly samples the right-handed and left-handed 3_{10}-helix region, whereas the presence of L-Pro or D-Pro generally favors the formation of turns or inverse turns [21,26,35].

The CPPs of general sequence c[YpwFXaa] have been prepared from the corresponding linear pentapeptide precursors, obtained in turn by standard solid phase peptide synthesis, using a Wang resin, Fmoc-protected amino acids, and *N*,*N*′-dicyclohexylcarbodiimide/HOBt as coupling agents [36]. The cleavage from the resin was obtained by treatment with trifluoroacetic

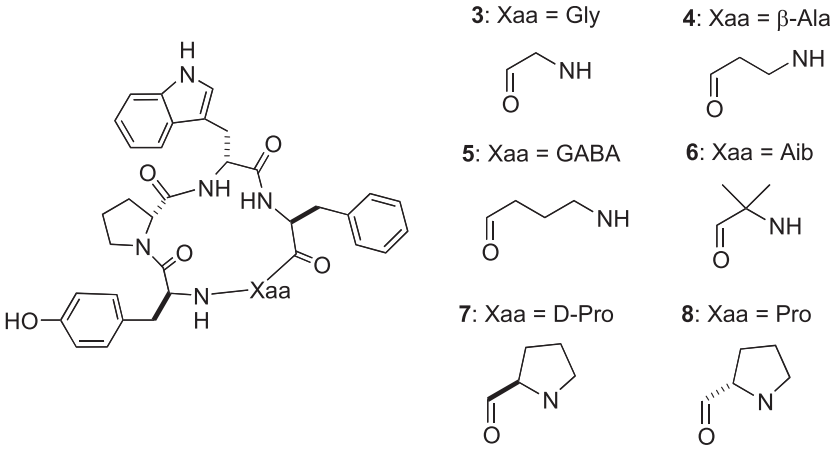

Fig. 2. Structures of the cyclopeptides c[YpwFXaa].

acid in the presence of scavengers, and the resulting linear peptides were subjected to in-solution cyclization with diphenylphosphorylazide (DPPA). The crude CPPs were purified by flash chromatography over silica gel, and using semipreparative RP-HPLC, and were characterized by analytical HPLC, ES MS, and ^{1}H-NMR. Yields after purification, purities and mass characterizations are reported in Table 1.

To determine the affinities towards the MORs, we performed displacement binding assays for compounds **3**–**8** and for the potent MOR-selective agonist DAMGO (H-Tyr-D-Ala-Gly-*N*-MePhe-glyol) as a reference compound. The peptides were incubated with rat brain membrane homogenates containing the receptors, using [^{3}H]DAMGO as a μ-specific radioligand [20] The K_i and IC_{50} values are reported in Table 1. In general, the peptides showed a concentration-dependent displacement of [^{3}H]DAMGO. Most of the peptides showed scarce receptor affinities; in particular, the introduction of longer, flexible amino acid spacers in compounds **4** and **5** led to a decrease of the K_i and IC_{50} values with respect to compound **3**. Apparently, a longer distance between the strategic pharmacophores of Tyr1 and Phe4 is not optimal for binding the receptor.

On the other hand, the introduction of spacers capable of reducing cyclopeptide flexibility is expected to influence OR affinities, depending on the precise conformation adopted by the whole molecule, albeit an improper size, nature, etc. of the conformation-controlling residue could obstruct efficient binding.

Interestingly, whereas the introduction of Aib and D-Pro gave compounds **6** and **7**, respectively, with a lower receptor affinity, the introduction of L-Pro gave compound **8,** which retained a moderate ability to bind the receptor, with K_i and IC_{50} in the 10^{-7} range (Table 1).

Conformational analysis of compounds 3, 7 and 8 in solution

Compound **3**, *c*[YpwFG], can be attributed an LDDLL or an LDDLD chirality, as Gly5 can act both as an L-residue and a D-residue. Therefore, we decided to investigate and compare the in-solution conformational features of compound **3**, compound **7**, *c*[YpwFp], which shows LDDLD chirality, and compound **8**, *c*[YpwFP], having LDDLL chirality, by spectroscopic and molecular dynamics (MD) analyses.

In spite of the moderate or scarce MOR affinities, the comparison of the in-solution structures of compound **3** with the structure of compound **7**, which is very poorly active towards the MOR, and compound **8**, which maintained some activity, being almost two orders of magnitude more active than the latter, could furnish useful clues on the biologically active structure of this class of atypical peptides. Also, the introduction of further conformational constraints in compounds **7** and **8** by changing the Gly to D-Pro or L-Pro should reduce the risk of ambiguous structures.

We could not perform experiments in water, because the peptides were practically unsoluble. Many peptides or peptidomimetics of interest described in the literature are not highly soluble in water, and have been studied experimentally in organic polar environments, in particular dimethylsulfoxide (for a leading reference on the use of dimethylsulfoxide as a biomimetic medium for the NMR of opioid peptides, see [37]). Accordingly, the NMR experiments on the lipophilic cyclopeptides were conducted using standard techniques at 400 MHz in dimethylsulfoxide-d_6.

For compound **3**, ^{1}H-NMR revealed a single set of resonances, suggesting conformational homogeneity or a fast equilibrium between conformers [21,26]. Variable temperature (VT)-^{1}H-NMR experiments (supplemen-

tary Table S1) in dimethylsulfoxide-d_6 gave the following $\Delta\delta/\Delta t$ values (p.p.b./K): TyrNH, −4.8; PheNH, −5.3; GlyNH, −1.4; D-TrpNH, −1.5. As there is a certain difference between the temperature coefficients, it is possible to hypothesize a conformational preference for a conformation in which GlyNH and D-TrpNH are involved in hydrogen bonds ($\Delta\delta/\Delta t$ of GlyNH and D-TrpNH < 2 p.p.b./K) [38].

Finally, 2D-ROESY in dimethylsulfoxide-d_6 furnished, apart from the obvious correlations, several diagnostic cross-peaks. The absence of $H\alpha_i$–$H\alpha_{i+1}$ cross-peaks was used to exclude the presence of *cis* peptide bonds. The observation of strong ROESY cross-peaks between Tyr1Hα and both D-Pro2Hδ was also used to infer a *trans* Tyr1–D-Pro2 amide bond. The data derived from NMR were analyzed by restrained MD, using nongeminal interproton distances as constraints, and structures were optimized with the AMBER force field [39]. The low-energy conformation with the lowest deviations from NMR data is shown in Fig. 3. This structure does not confirm the occurrence of explicit hydrogen bonds, probably because of the occurrence of a fast equilibrium between different geometries, whose average in the NMR time scale gives the structure determined by ROESY analysis [21,23]. Concerning the orientations of the side chains, ROESY data accounted for a *trans*, g^+, and g^- orientation of Tyr, D-Trp, and Phe, respectively.

To investigate the inherent flexibility of the cyclopeptide backbone [21], we performed a 5.0 ns unrestrained MD simulation in explicit water. During the simulations, the cyclopeptide oscillated from a preferred conformation **A**, matching the VT-NMR temperature coefficients (Fig. 4, supplementary Table S1), characterized by a type II β-turn centered on Tyr1-D-Pro2, and an inverse γ-turn centered on Phe4, to a secondary conformation **B** showing an inverse type I

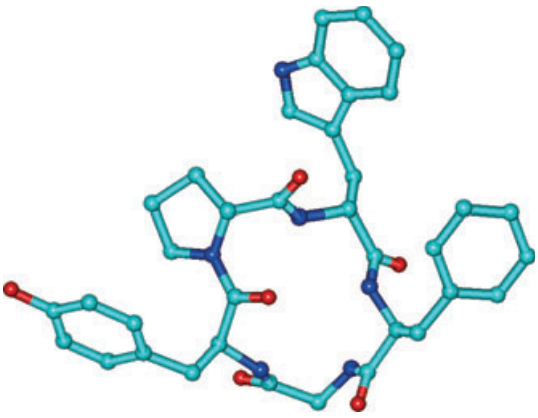

Fig. 3. Minimized conformation of compound **3** calculated by restrained MD with the lowest internal energy and the least number of violations of ROESY data.

β-turn centered on D-Pro2-D-Trp3, and a γ-turn on Gly5 (Fig. 4). During the simulations, the more frequently populated rotamers observed for Tyr, D-Trp and Phe were in agreement with ROESY data.

The conformational analysis of compound **7**, *c*[YpwFp], was performed in a similar way as for compound **3**. The structural data obtained from NMR analysis reproduced most of the features of compound **3**. ^{1}H-NMR revealed also the presence of a extra set of small signals in the NH region, indicating a small population (< 5%) of conformers in slow equilibrium with the main species. This secondary population very likely corresponds to conformers containing at least one *cis* peptide bond preceding Pro, in agreement with other CPPs containing two Pro residues reported in the literature [26]. Because of the scarce intensity of the secondary set of signals, the conformational analysis was conducted only on the predominant conformer.

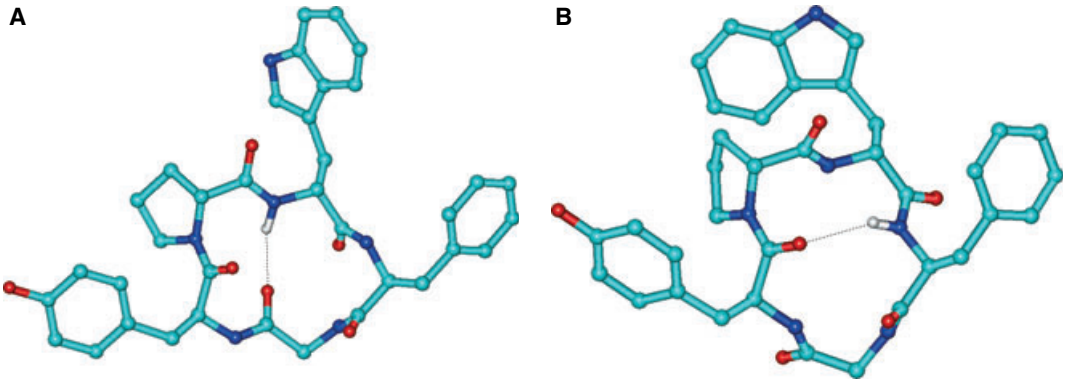

Fig. 4. Conformations **A** (left) and **B** (right) of compound **3** observed from unrestrained MD simulations in explicit water.

The data derived from 2D-ROESY analysis, indicating an all-*trans* disposition of the ω-bonds, were utilized for performing restrained MD, and the structures were optimized with the AMBER force field. The representative conformation with the lowest energy and the least violations of restraints is shown in Fig. 5.

This structure shows an explicit hydrogen bond between Tyr1CO and Phe4NH, and a conformation in which the residues D-Pro2-D-Trp3 occupy positions $i + 1$ and $i + 2$ of a inverse type I β-turn, whereas Gly5 occupies position $i + 1$ of a γ-turn. The involvement of PheNH in a hydrogen bond could not be deduced on the basis of simple VT-NMR analysis.

The structure of compound **7** very closely resembles the structure of compound **3B** (Fig. 4). The mirror image of the conformation of compound **7**, c[YpwFp], which is characterized by LDDLD chirality, is perfectly compatible with that reported in the literature for c[GPfAP] and other CPPs [26,40] in solution, characterized by a type I β-turn on Pro2-D-Phe3, and a inverse γ-turn on Pro5. The latter peptide has DLLDL chirality, opposite to that of compound **7**, and contains two Pro residues in the same positions, 2 and 5, as in compound **7**, and Gly1, serving as a D-residue [26].

The unrestrained MD simulation in explicit water confirmed the strong stability of the conformation. At intervals, the simulation revealed also the presence of a γ-turn on D-Pro5. The low $\Delta\delta/\Delta t$ value observed for D-TrpNH could, in principle, be causedby a population of conformers showing an alternative hydrogen-bonded structure. The same CPP model, c[GPfAP], has also been reported to adopt a inverse type II β-turn centered on Gly1-Pro2 and a γ-turn centered on Ala4 in the crystal state [26]. However, for the compound **7**, no trace of any turn centered on Gly1-Pro2 was observed during the time selected for the simulation.

Finally, we analyzed the conformation of compound **8**, *c*[YpwFP]. As for compound **7**, ^{1}H-NMR in dimethylsulfoxide-d_6 revealed a more abundant and a largely minor set of resonances, which was neglected. Concerning the 2D-ROESY analysis in dimethylsulfoxide-d_6, the presence of a clear cross-peak of type $H\alpha_i$–$H\alpha_{i+1}$ between Phe4Hα and Pro5Hα was considered to be indicative of a *cis* Phe4-Pro5 ω-bond. The other Pro-preceding peptide bond was considered to be *trans*, because of the presence of strong cross-peaks between Tyr1Hα and both D-Pro2Hδ. The interproton distances deduced from ROESY analysis were utilized as constraints for performing restrained MD simulations. The large majority of the calculated structures of compound **8** did not show any significant violation of the restraints associated with backbone protons, and were well ordered. The representative structure reported in Fig. 6 is consistent with an inverse type I β-turn centered on D-Pro2-D-Trp3. VT-^{1}H-NMR analysis in dimethylsulfoxide-d_6 confirmed the involvement of PheNH in a very strong hydrogen bond (supplementary Table S1).

Finally, the unrestrained MD simulation performed in explicit water confirmed the extreme stability of the conformation.

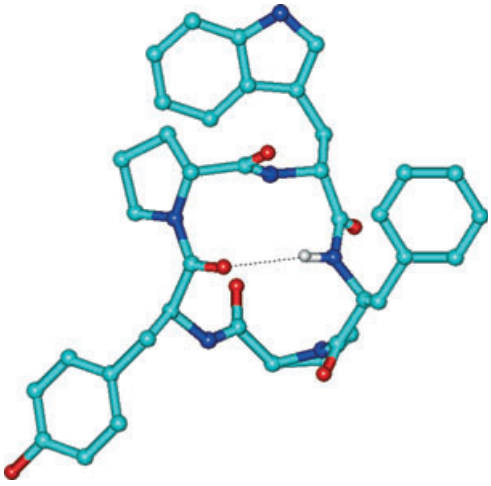

Fig. 5. Representative minimized conformation of compound **7** calculated by restrained MD with the lowest internal energy and the least violations of restraints.

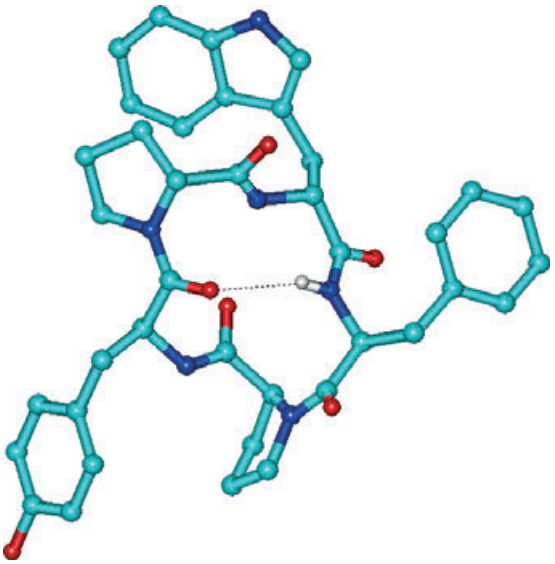

Fig. 6. Representative conformations of compound **8** calculated by restrained MD and minimized with the lowest internal energy and the least violations of restraints (no significant violations of the restraints associated with backbone protons).

Molecular docking

The potential receptor-binding modes of the CPPs have been analyzed by molecular docking. As reported in the literature, it is manifest that for most opioid ligands the construction of ligand–receptor complex models began with the assumption that the protonated amine interacted electrostatically with Asp147 in transmembrane helix (TMH) III (Fig. 7) [28,41,42]. In several cases, ligands have been manually docked into the receptor cavity in order to place the protonated amine close to the conserved Asp. Compound **3** does not contain any ionic functionalities; therefore, an alternative approach must be undertaken. The main binding force towards the receptor would comprise hydrophobic and hydrogen-bonding interactions.

Because of the absence of a leading interaction, the docking process was performed by AUTODOCK [30], because it is a truly exhaustive docking program that explores the full pose and conformational space of the protein–ligand complex using a very fine grid. Following the creation of an appropriate interaction model of compound **3** (the most active analog), using the 'blind docking' approach [31,32], compound **3** and its analogs were docked into the approximate binding site previously found using a finer grid ('refined docking'), and the resulting orientations were then equilibrated by MD.

The conformations resulting from the 'blind docking' run were clustered, and most of them (up to 91% of the docking solutions) were found to be located in the channel pore between TMH III, TMH V, TMH VI, TMH VII, and the extracellular loop (EL)-2. The residues belonging to the binding site within 3 Å from the ligand are those corresponding to Tyr148, Met151 and Phe152 (TMH III), Lys233 and Phe237 (TMH V), Ile296, Val300, Lys303 and Thr307 (TMH VI), Trp318 and Ile322 (TMH VII) and Thr218, Leu219 and Phe221 (EL-2) of MOR.

The location of this binding site was then used as the starting point for the second docking run. In this case, the use of a finer grid resolution allowed a superior evaluation of ligand–receptor interactions, with lower (improved) docked energies being obtained with respect to the previous step. The cyclopeptide conformations resulting from this 'refined docking' study were clustered and, after a visual inspection of the docking results, the solutions could be divided into two main orientations, orientation 1 and orientation 2, based on the position of the ligand inside the binding pocket and on the residues that were within 5 Å of the ligand (for comparative side/top views of orientation 1 (A–C) and orientation 2 (D–F) of the different CPPs, see also supplementary Fig. S5). In the following sections a detailed discussion to define the best orientation in terms of ligand-receptor binding efficacy is presented.

Orientation 1

The location of compound **3** in this orientation shows the Tyr1 group pointing towards a hydrophobic pocket composed mainly of the aromatic residues Tyr148, Phe237, Phe241 and Trp293 (Fig. 8A). By

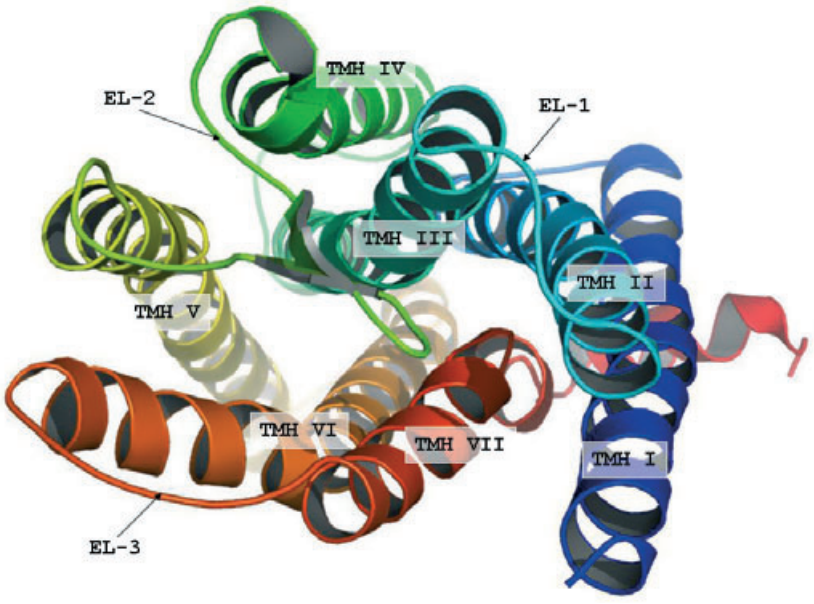

Fig. 7. Cartoon representation of the TMHs and ELs of MOR, top view from the extracellular surface, colored by secondary structure succession, and prepared using PYMOL [42].

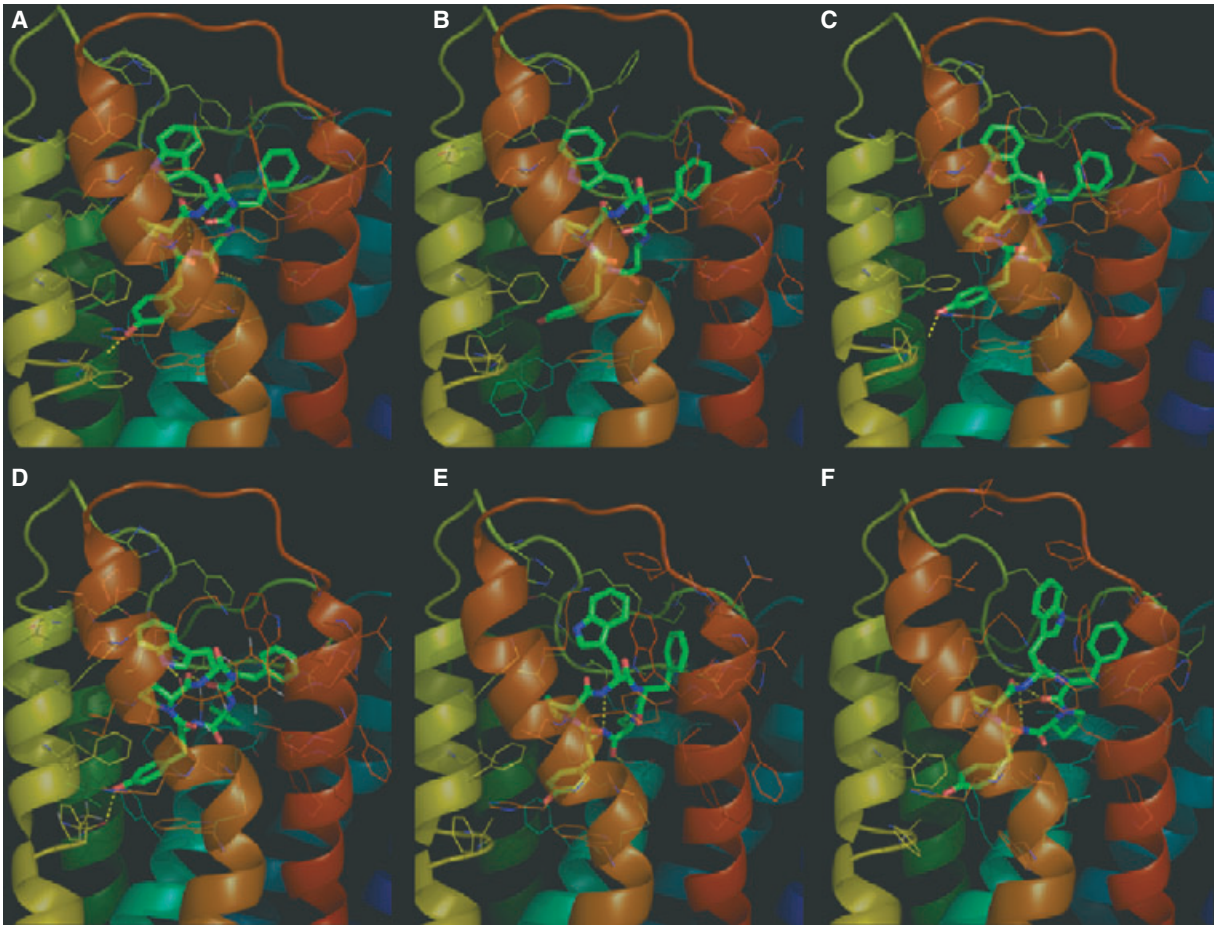

Fig. 8. Side views of compounds **3–8** in orientation 1 [ordered from (A) (compound **3**) to (F) (compound **8**) and rendered as sticks] docked into the binding site of MOR using AUTODOCK, except for compound **8**, which was manually docked (see text). The MOR is shown in cartoon representation and colored by secondary structure succession, the residues within 5 Å of compounds **3–8** are shown as wireframe, and hydrogen bonds are shown as yellow dashed lines. All of the figures were prepared using PYMOL [42].

comparison with Fig. 4, it appears that this disposition within the receptor cavity seems to be similar to the preferred conformation adopted in solution. The ligand–receptor complex is stabilized by four hydrogen bonds: two between the backbone oxygen of Gly5 and $O^{\delta 1}$ and $O^{\delta 2}$Asp147 (2.90 and 2.78 Å respectively), the only residue from THM III within 5 Å of compound **3**, one between $O^{\gamma 1}$ of Thr218 (EL-2) and the backbone oxygen of Phe4 (2.94 Å), and one between the hydroxyl oxygen of the Tyr1 group and OAla240 (TMH V) of 2.66 Å.

The close proximity of Tyr1 to THM VI would allow hydrogen bonds to be formed here with the backbone carbonyl, which may stabilize the position of this group. As stated above, in this orientation, compound **3** is stabilized also by many 'stacking' or π–π interactions between the aromatic moieties of Tyr1 and Phe4 and the side chains of Phe237, Phe241 and Trp293 (Trp1), Trp218 and Phe221 (Phe4). Trp3 is involved in a cation–π interaction with Lys303 (TMH VI), whereas the other positive residue within 5 Å of the ligand (Lys233, belonging to TMH V) does not show any evident interaction with compound **3**.

The docking results for the other cyclopeptides (with the exception of compound **8**, see below) give rise to a binding conformation very close to that obtained for compound **3** (Fig. 8; see supplementary Fig. S5). Compounds **4**–**6** show the poorer binding score values, a result that can be related to an inadequate interaction with the binding site. In this orientation, compound **4** is characterized by a shift (rotation) of Tyr1 away from TMH V and TMH VI, giving rise to the breaking of the hydrogen bonds with Ala240 and Asp147, and by the presence of only one lengthened hydrogen bond, between OPhe4 and $O^{\gamma 1}$Thr218 (EL-2) of 3.52 Å. Tyr1 is always inserted inside the aromatic

cluster and Phe4 is stabilized by a π–π interaction with Trp318, but Trp3 does not show any cation–π interaction with Lys303.

In compounds **5** and **6**, HOTyr1 is capable of interacting again with OAla240 (2.52 and 2.81 Å, respectively). These structures are stabilized also by hydrogen bonds between NGABA5 and OCys217 (for compound **5**, 2.20 Å) and between OPhe4 of compound **6** and $O^{\gamma 1}$Thr218 of 2.42 Å, but the increasing size of the Xaa5 residue still prevents the interaction with Asp147. In compound **7**, where Xaa5 is a D-Pro residue, the interaction with Asp147 is restored, by means of the carbonyl oxygen of D-Pro5 (2.20 Å), and supported by a hydrogen bond between NTyr1 and $O^{\gamma 1}$Thr218 (3.30 Å). Trp3 is again involved in a cation–π interaction with Lys303 (TMH VI), and Tyr1 is now stabilized by two π–π interactions with the aromatic side chains of Phe237 and Trp293.

For compound **8**, the one showing the second-best affinity (Table 1), none of the docking solutions can be clustered in an orientation comparable to orientation 1, a result at first attributable to the excessive steric hindrance of the Pro5 residue. This observation is not completely surprising. For compounds **3** and **7**, the structures in orientation 1 (Fig. 8A,E) roughly correspond to the preferred conformations in solution, whereas compound **8** in solution shows a quite different shape from that adopted by the other peptides. Concerning compounds **4** and **5**, the introduction of longer, flexible Xaa5 spacers is expected to increase the overall conformational freedom and the adaptability to the receptor-binding pocket.

Consequently, compound **8** was manually docked inside the MOR binding pocket, using the orientation of compound **3** as a template. This results in a conformation characterized by the presence of three hydrogen bonds between $O^{\gamma 1}$Thr218 and NTyr1, OPhe4 and OPro5 (of 2.77, 2.96 and 3.26 Å, respectively) and by two π–π interactions between Tyr1 and Phe237, and Trp3 and Phe221. Tyr1 is always inserted inside the aromatic cluster, but lacks the hydrogen bonds with Ala240 and Asp147 (Fig. 8F). The binding site is completed by Asp216, Val300, His319 and Ile322, which are located within 3.5 Å of compound **3**, although no particular interactions are implicated between these residues and the ligand. The complete amino acid composition of the binding site is reported in supplementary Tables S5–S11.

Orientation 2

In this orientation, the one showing the best binding energy scores for all the studied peptides, compound **3** is located in a cavity-like region inside the channel pore (Fig. 9A), reversed as compared to orientation 1, and shifted approximately 3.3 Å away from TMH VI, which brings Ala240 (TMH V) and His297 (TMH VI) to a position far away from the ligand. The repositioning of compound **3** also means that EL-3 is now within 5 Å of the ligand.

The overall shape of the receptor-bound structure of compound **3** in orientation 2 strongly differs from that in solution (Fig. 4), also in terms of backbone conformation. Compound **3** is directed towards the bottom of the binding site by its D-Trp3 group and stabilized by the formation of six hydrogen bonds: a bidentate hydrogen bond between $O^{\delta 1}$ and $O^{\delta 2}$ of Asp147 (TMH III) and the nitrogen atom of the D-Trp3 indole ring (3.15 and 3.06 Å, respectively), two contacts between the backbone carbonyl oxygen of the Tyr1 group and $O^{\varepsilon 2}$Glu229 (TMH V, 3.22 Å) and OThr220 of 3.30 Å, and the last bidentate hydrogen bond between the $O^{\varepsilon 1}$ and $O^{\varepsilon 2}$Glu310 (EL-3) and the OH-Tyr1 of compound **3** (3.04 and 3.38 Å, respectively). In this orientation, Tyr1 and Phe4 are surrounded by Phe221 and Trp318, and the D-Trp3 is now located inside the hydrophobic pocket that in orientation 1 was occupied by Tyr1 and composed mainly of the aromatic residues Tyr148, Phe152 and Phe237.

Thr218, Leu219, Lys233, Lys303, Thr307 and His319 are located within 3.5 Å of the CPPs and complete the binding site walls, although no particular interactions are implicated between these residues and the ligand. Again, the complete amino acid composition of the binding site is reported in supplementary Tables S5–S11.

The docking results for the other CPPs give rise to a binding mode similar to that obtained for compound **3** (Fig. 9 and supplementary Fig. S5). The analysis of the docking solutions for compound **4** shows the absence of contacts with both Asp147 and Glu310, and the presence of only one hydrogen bond between the carbonylic oxygen of D-Pro2 and $O^{\gamma 1}$Thr218 of 2.69 Å, a situation common also to compound **5**, stabilized by the formation of two hydrogen bonds between $O^{\gamma 1}$Thr218 and OPro2 and NPhe4 of 3.26 and 3.45 Å, respectively. This behavior is partially verifiable in compounds **6** and **7** where the hydrogen bond with Asp147 is still absent but there is re-formation of the contact between HOTyr1 and $O^{\varepsilon 2}$Glu310 with distances of 2.63 and 2.69 Å (for compounds **6** and **7**, respectively). In compound **7**, the conformation is also stabilized by a cation–π interaction between Tyr1 and Lys303.

The binding mode observed for compound **3** in orientation 2 is completely restored in compound **8**,

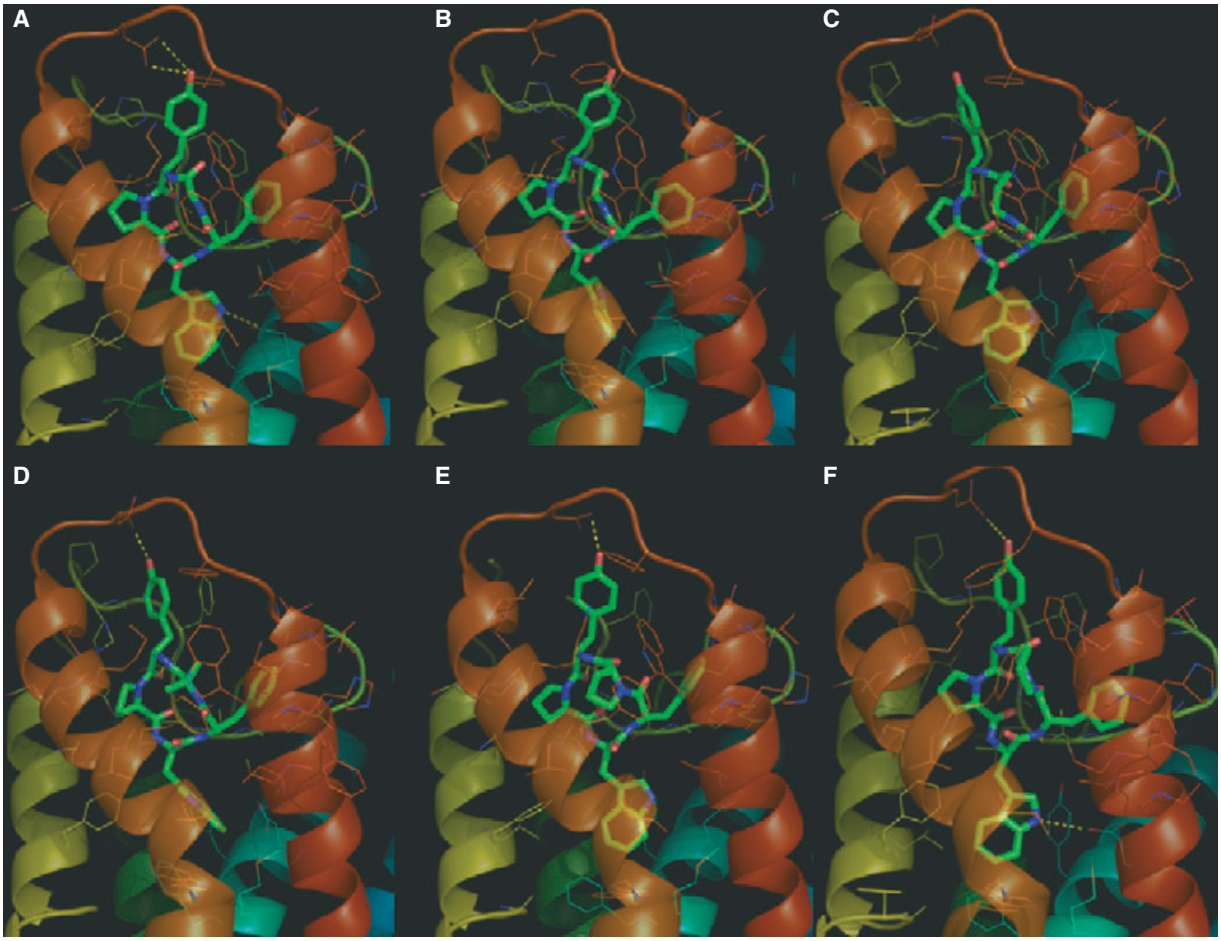

Fig. 9. Side view of componds **3–8** in orientation 2 [ordered from (A) (compound **3**) to (F) (compound **8**) and rendered as sticks] docked into the binding site of MOR using AUTODOCK. The MOR is shown in cartoon representation and colored by secondary structure succession, the residues within 5 Å of compounds **3–8** are shown as wireframe, and hydrogen bonds are shown as yellow dashed lines. All of the figures were prepared using PYMOL [42].

with the formation of three out of five hydrogen bonds: one between $O^{\delta 2}$Asp147 and the nitrogen atom of the D-Trp3 indole ring of 3.34 Å, one between NPhe4 and $O^{\gamma 1}$Thr218 of 3.23 Å, and one between $O^{\varepsilon 2}$Glu310 and OHTyr1 of compound **8** (3.23 Å). In this orientation, D-Trp3 of compound **8** is surrounded by Phe237 and Trp293, and Tyr1 is involved in a cation–π interaction with Lys303.

Hybrid QM/MM induced fit

The two main orientations of all the peptides were then further analyzed through hybrid QM/MM geometry optimization [33,34]. There are several reasons for combining docking techniques with other computational methods: estimation of the quality of the scoring functions, re-ranking of the structures generated by docking, simulation of the structural adaptations that occur in a receptor upon ligand binding, a more detailed description of the binding mode of the ligand, and, in the case of QM methods, a complete description of reaction mechanisms and electronic properties. Hybrid QM/MM methods have become a standard tool for the characterization of complex molecular systems. The basic idea of these methods is to treat that part of the system that undergoes the most important electronic changes upon binding a substrate quantum mechanically, and the rest of the system by traditional molecular mechanics.

The protein environment is influenced by a ligand bound to the binding site ('induced fit'), and a QM/MM optimization of the resulting complexes gives a more accurate description of the electronic and steric properties of the ligand. As QM calculations on whole protein systems are computationally very demanding, we chose a QM/MM approach for

the optimization of the two solutions obtained by docking, using the program package GAUSSIAN 03 [43]. First, the relevant binding conformations of the MOR–substrate system resulting from the molecular docking runs were equilibrated for 1.2 ns by MD, at constant temperature and pressure in a periodic cubic box, using the TIP3P model for water molecules. The systems were subsequently optimized using the combined QM/MM approach, with a flexible receptor environment that allows the simulation of the adaptation of the receptor upon ligand binding. This procedure give rise to a rearrangement of the residues forming the binding site around the ligand ('induced fit'), leading to the situation shown in Fig. 10 for compounds **3**, **7** and **8** in both orientations 1 and 2 (results for the remaining CPPs are not shown; see also supplementary Tables S7–S9).

The compound **3** binding site optimization lead to a small difference in the residue geometry with respect to the starting conditions, with all-atoms rmsd values of 1.08 and 1.21 Å for orientations 1 and 2, respectively. The numbers of hydrogen bonds and residues that make contact with compound **3** is almost unaffected: the ligand in orientation 2 moves towards TMH III and EL-2, making new contacts with residues belonging to TMH VI. Phe221, Trp318 and His319 remain almost unaffected by the binding with compound **3**, whereas Asp147 and Glu310 move towards D-Trp3 and Tyr1, respectively, to improve the hydrogen bond geometry.

The most significant variation in orientation 2 involves the Trp293 residue of TMH VI, which reorients its indole side chain, leading to a better π–π interaction. The same effect can be observed for Phe237

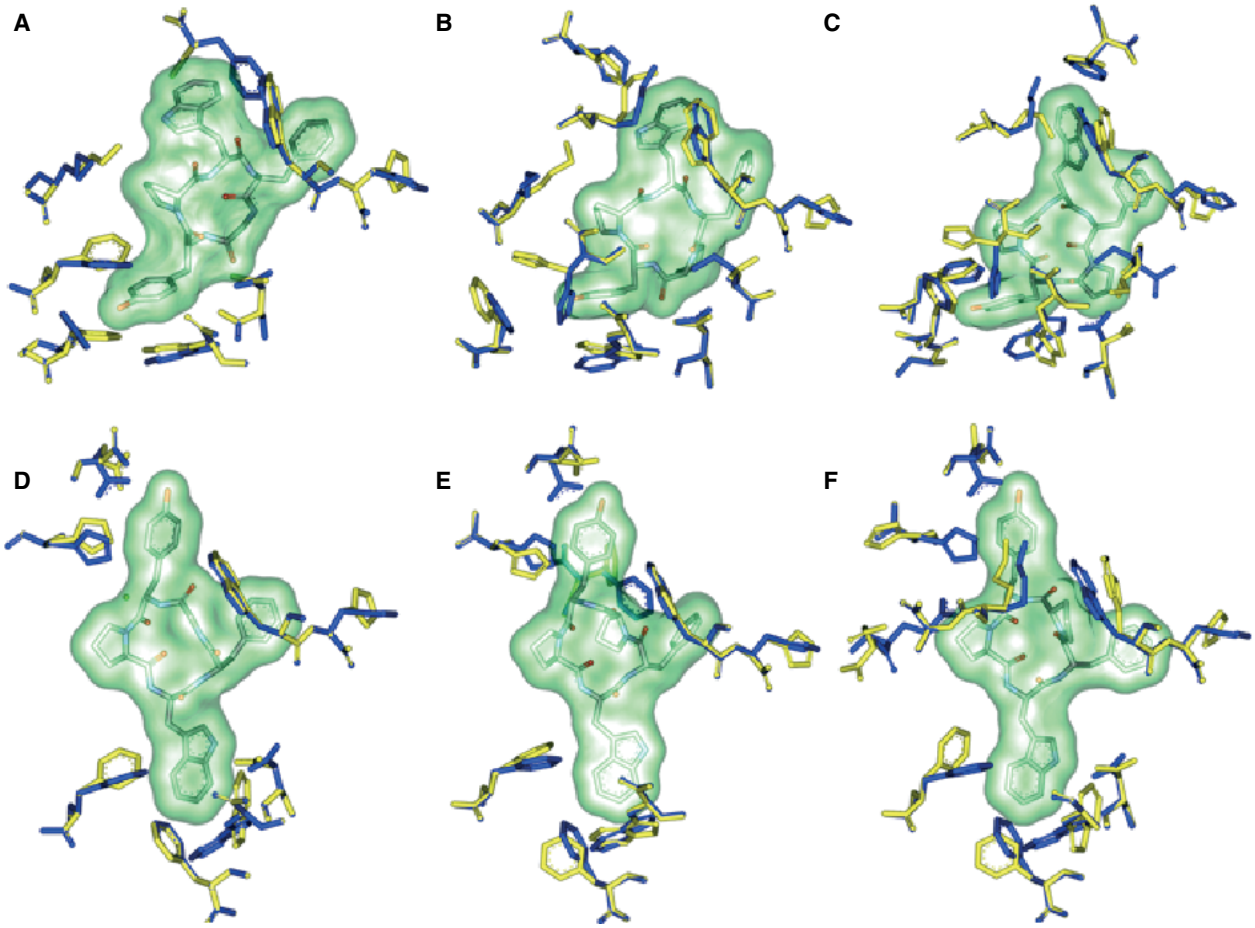

Fig. 10. Details of the QM region used in the QM/MM optimization of the complex formed between the MOR and the bioactive conformations of compounds **3**, **7** and **8** in orientation 1 (A–C) and orientation 2 (D–F). Yellow sticks: MOR residue positions after the QM/MM optimization results. Blue sticks: MOR residues included in the QM part in their initial conformation. The ligands after the QM/MM optimization are represented by sticks (CPK color) and enclosed by their solvent accessible surface (SAS).

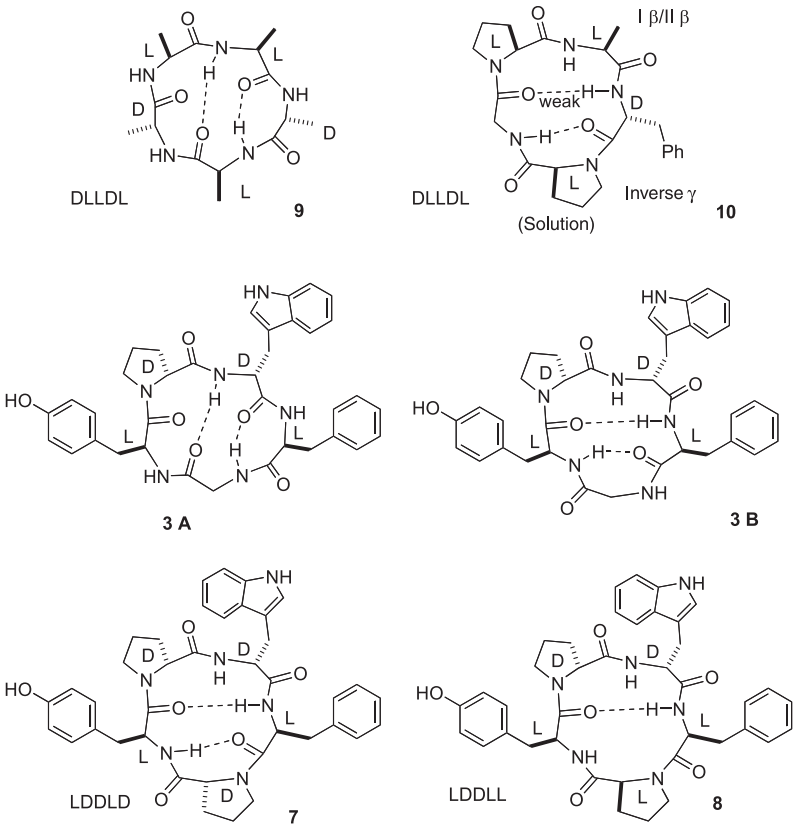

Fig. 11. Comparison of the secondary structure elements determined for compounds **3**, **7** and **8**, and for the model CPPs, compounds **9** and **10**.

and Phe241, but in these cases the flip of the aromatic side chains is not so great as for Trp293.

The QM/MM binding site optimization of compound **7** shows a pattern of residue movements superimposable on those observed for compound **3**, leading to the smallest difference in the residue geometry with respect to the starting conditions, with all-atoms rmsd values of 0.85 and 1.12 Å for orientations 1 and 2, respectively. In orientation 1, the movements of the binding site residues due to the ligand binding are mainly represented by a series of modest rotations of the Tyr148, Phe237, Phe241 and Trp293 lateral chains, in order to surround Tyr1. Asp147 remains almost unchanged by the ligand binding, and the positively charged residues Lys233 and Lys303 point towards D-Trp3, whereas Ile322 and His297 move far away from the ligand to lower the steric hindrance with D-Pro5 and Tyr1, respectively. In orientation 2, the binding site require a smaller amount of movement to adapt its structure to compound **7**. In this case, the Lys residues, Trp293 and Asp147 do not move from their initial positions, whereas Glu310 moves towards Tyr1 to improve the hydrogen bond geometry.

As stated above, the analysis of compound **8** in orientation 1 started from the manually docked structure because of the absence of a solution matching this orientation in the automated docking run, and this behavior can be explained by taking into account the results obtained in the QM/MM run. The binding of compound **8** in orientation 1 leads to extensive variations in the 3D structure of the binding site with respect to the starting conditions (with an all-atoms rmsd of 1.21 Å), in particular near the Pro5 residue, with a wide movement of the Asp147, Tyr148, Trp293 and Ala323 lateral chains. In orientation 2, compound **8** shows the same behavior as compound **3**, but with more important variations in the zone near Trp293, composed mainly of Phe237 and Phe241, and a small reorientation of the Trp293 indole lateral chain, suggesting less activation of the receptor with respect to compound **3**.

Afterwards, the residue movements resulting from the induced fit analysis lead, for compound **3**, to a cavity geometry characterized by values of the exposed area of $\sim$ 770 Å^2 and $\sim$ 780 Å^2 for orientations 1 and 2 respectively, but with a smaller contact area for orientation 2 with respect to orientation 1 ($\sim$ 597 Å^2 and $\sim$ 537 Å^2 for orientations 1 and 2, respectively). This behavior is common to all of the studied CPPs, leading to a smaller deformation of the binding site and

then to greater stability of the cyclopeptide–receptor complex.

Discussion

CPPs are expected to be relatively conformationally rigid. However, despite the constrained structure, CPPs generally exhibit a remarkable degree of residual flexibility. In the previous section, MD simulations indicated that the opioid CPP agonist compound **3** in solution can adopt a couple of different β/γ-turn conformations stabilized by alternative hydrogen bonds, whereas compounds **7** and **8** show more rigid structures, characterized by a single main conformation. Interestingly, whereas LDDLD compound **7** adopts an all-*trans* ω-bond conformation, in agreement with similar CPPs reported in the literature, the unprecedented LDDLL compound **8** adopts a one-*cis*-four-*trans* ω-bond conformation, the *cis* peptide bond being the one preceding Pro5 (Fig. 11).

It is generally accepted that the overall conformation of CPPs depends, for the most part, on the stereochemistry array. The structure of compounds **3** (LDDLL or LDDLD), **7** (LDDLD), and **8** (LDDLL) can be tentatively compared to that of LDDLL or LDDLD cyclopentaalanine models [27]. Therefore, compounds **3**, **7** and **8** can be compared either to the model c[AaaAA], which exhibits LDDLL chirality, or to the mirror image of the model c[aAAaA] (compound **9**) as well as of the structurally related $\alpha_v\beta_3$-integrin inhibitor c[fVRGD] (generally reported as c[RGDfV]) [27], both of which show DLLDL chirality, the opposite of LDDLD (Fig. 11).

The structure of the LDDLL model c[AaaAA] shows a well-defined type II β-turn on Ala1-D-Ala2. On the other hand, the diastereomeric LDDLD model c[aAAaA] (compound **9**) still maintains a type II inverse β-turn on D-Ala1-Ala2, and also a γ-turn on D-Ala4. As a consequence, conformation **A** of compound **3** can be easily rationalized.

However, Pro-containing cyclopeptides usually manifest specific structural features with respect to the other cyclopeptides, mainly due to the increased probability of showing a *cis* conformation of the ω-bond preceding Pro, and the strong tendency to stabilize turn structures.

In particular, Pro tends to occupy the $i + 1$ position of a β-turn or of a γ-turn. Indeed, DLLDL Pro-containing CPPs such as c[GPAfP] [26] (compound **10**), D-Gly(Set)-PFaV [40], c[GPSaP], c[GPAaP] or c[fPGaP] showed all-*trans* peptide bond structures characterized by a preference for a type I/type II β-turn centered on the residues in positions 2 and 3, accompanied by a inverse γ-turn on the residue in position 5. Apparently, the presence of a Pro in position 2 of compound **3** is responsible for the occurrence of the second conformation, conformation **B** (Fig. 11).

Accordingly, the mirror image of the conformation of the two-Pro-containing compound **7** determined by restrained MD perfectly matches the conformational aspects of the above described DLLDL CPP models containing two Pro residues (see also Results).

In contrast, the chirality sequence and conformation of compound **8** do not match other two-Pro-containing CPPs reported in the literature. In general, the competition between structures having a *cis* Xaa-Pro peptide bond versus β-turn or γ-turn structures in which the Xaa-Pro peptide bond must necessarily adopt a *trans* conformation mainly depends on the chirality of the other residues, rather than on their nature. For instance, it has been documented that the introduction of an L-Ala in position 1 of c[GPGaP] destabilized the original conformation, giving a mixture of an all-*trans* and a one-*cis* form in the Ala–Pro ω-bond [26]. In a similar way, the introduction of an L-Ala4 in c[GPfaP] in place of the D-residue lead to the coexistence in solution of four different structures containing all possible combinations of *trans/cis* ω-bonds preceding both Pro2 and Pro5 (*cis/cis*, *trans/trans*, *cis/trans*, *trans/cis*) [26]. Remarkably, compound **8** shows a single one-*cis*-four-*trans* ω-bond conformation, instead of a mixture of different *cis/trans* structures.

Despite the presence of distinct secondary structure elements, both conformations **3A** and **3B** show rather similar display of aromatic side chains (Fig. 4), the main difference being the distance between Tyr1 and Phe4 side chains. In particular, conformation **A** observed in solution for compound **3** is in agreement with the structural requirements reported in the literature for good activity and selectivity towards MORs. Conformational analysis of EM-1 [44], morphiceptin [45], enkephalins [46] and their derivatives [28,47–51] have established that a *trans* χTyr1 angle, and a relatively large separation (about 11–13 Å) of the Tyr phenolic ring with a second aromatic pharmacophore, are necessary for optimal interaction with MORs [52]. In addition, a g^- orientation has been recommended for χTrp3 [47], whereas a preferential g^- conformation of Phe4 has been hypothesized on the basis of the good receptor affinity shown by endomorphin analogs containing a (2*S*,3*S*)-β-MePhe in position 4 [53].

Concerning compound **3**, in conformation **A** the aromatic side chains of Tyr1 and Phe4 are about 12 Å from each other, and their χ angles are *trans* and g^-, whereas the g^+ orientation observed for D-Trp3 is compatible with the reversal of the absolute configuration with respect to EM-1. In essence, compound **3A**

seems to be almost superimposable on that of the potent MOR agonist JOM-6 (Fig. 12), whose interaction with OR has been the subject of intense investigation [50,51]. In particular, the key interaction between the ligand and the receptor was determined to be the ionic interaction involving the ligand's TyrNH and Asp147 of TMH III, as reported for several other opioid agonists [28,41].

The structural similarity seems to suggest that the two compounds could interact with the MOR in a similar way, the absence of ionic interactions being responsible for the lower affinity of compound **3** with respect to JOM-6 (K_I = 0.17 nM [50,51]). However, the correlation between the diverse biological activities of compounds **3**, **7**, and **8**, and their in-solution structures, discourages this assumption. Indeed, it is evident that whereas the pharmacophores of the two compounds are almost superimposable, the CPP backbone does not superimpose at all. In principle, the observed flexibility shown by compound **3** could account for the possibility of a CPP–receptor fit with a distorted conformation. However, the moderate receptor affinity shown by the less flexible compound **8**, which in solution adopts a different 3D structure with respect to compound **3**, requires the formulation of a different ligand–receptor interaction model.

As a consequence, the interactions between the CPPs and MOR have been investigated by molecular docking. The computations indicated that, in general, the CPPs can fit the receptor by adopting two different, opposite dispositions. The first model is similar to the model described for JOM-6, and shows a peptide disposition within the receptor cavity, orientation 1, very similar to the preferred conformation adopted in solution (Figs 8 and 12), whereas in the second model, the CPPs are located in the receptor with a reversed disposition, or orientation 2 (Fig. 9).

A comparison between orientations 1 and 2 of the most active cyclopeptide, compound **3**, reveals a different overlap to that of JOM-6 (Fig. 13). The aromatic ring of the Phe4 residues of compound **3** is completely superimposable on that of Phe3 of JOM-6, especially that of orientation 2. Orientation 1 is able to obtain an excellent superimposition of Tyr1, whereas orientation 2 is reversed, replacing Tyr1 with D-Trp3. But the main difference is evident when considering the superposition of the backbones: in orientation 2, the backbone is located in the same position with respect to that of JOM-6, whereas the backbone in orientation 1 is shifted by about 5 Å towards the bottom of the receptor cavity, leading to greater steric hindrance. For all the studied peptides, the shift of the cyclic backbone can also be related to the small difference in the docking score, giving rise to a situation where orientation 2 is favored over orientation 1.

These differences between the two orientations must be analyzed considering that: (a) the great majority of conformers were found in orientation 2; and (b) the binding energy of the conformations found for the first orientation were always near those found for the second one (the one showing the best docking score). As the lack of flexibility in the protein may influence the binding modes of the ligands, and the affinities and orientations may vary significantly from one solution to another, these results should be considered with care. In particular, the small difference in the docking score between the two orientations of the CPPs gives rise to a difficulty in the prediction of which one is the best orientation. It is worth noting that the binding site was found without imposing any

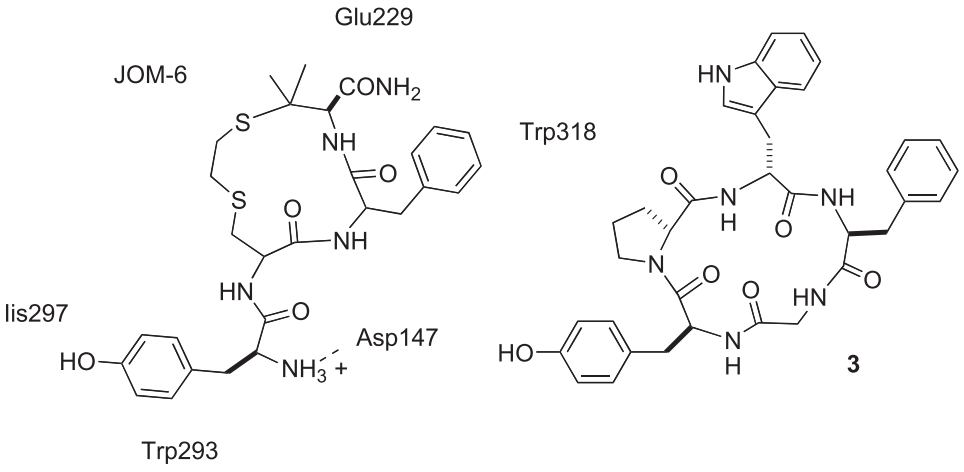

Fig. 12. Comparison of the receptor-bound structure of JOM-6 with the in-solution average structure of compound **3**.

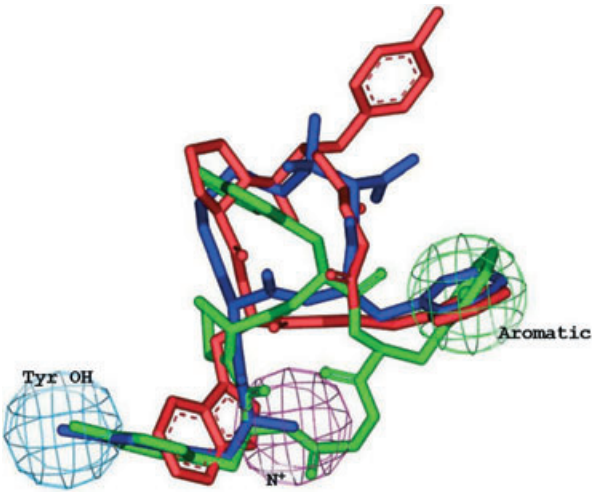

Fig. 13. Superimposition of the conformations of compound **3** in orientation 1 (green), and in orientation 2 (red), and JOM-6 (in blue), docked into the binding site of MOR. The three important pharmacophoric centers are shown.

constraint and in the absence of water molecules in the docking process.

Interestingly, whereas compound **3** and the analogs compounds **4**–**7** can fit the receptor in both orientations, compound **8** shows an exclusive preference for the second, reversed orientation 2. The docked structure of compound **8** in orientation 2 shows some structural differences in the Pro5 region with respect to the in-solution structure. In a similar way, the in-solution conformation of compound **3** has to be modified in order for it to fit the receptor. Compound **8** has a comparatively higher conformational rigidity; therefore, the modification of the in-solution conformation to fit the receptor has some consequences in terms of biological activity, and indeed compound **8** shows a lower activity than compound **3**.

The analysis of the correlation coefficients obtained between the calculated docking energies and the K_i or IC_{50} values demonstrates the better predictive power of orientation 2 with respect to orientation 1. This finding is confirmed by looking at the excellent statistical parameters obtained for the linear regression of ΔG_{dock} versus ΔG_{exp} for orientation 2 (Fig. 14).

It is important to emphasize that orientation 2 is characterized by several intense interactions, with Asp147, Glu310 and Trp318, that seem to be important for the activity improvement, in that they are present in both compound **3** and compound **8**, the two most active cyclopeptides. The proposed binding site is situated not far from the location previously identified by docking studies as the binding site for JOM-6 [50,51]. The importance of the key residues defining the binding pocket, and determined by site-directed mutagenesis, is confirmed also for this class of cyclopeptides. Despite the absence of the charged nitrogen, all of the studied CPPs show an interaction with Asp147. Furthermore, in orientation 2, the role played by Glu229 in the proposed EM-2 binding model [54] seems to be played by Glu310, because both residues are located at the entrance of the binding pocket, in a flexible loop structure, and therefore they are available for interaction with the ligands.

The two main orientations of the peptides were then refined through hybrid QM/MM geometry optimization. This procedure highlighted a further, strategic interaction between D-Trp3 and Trp293 of the CPPs in orientation 2. Obviously, this interaction is absent in the reversed orientation 1. The improved contact between D-Trp3 and Trp293 is of particular interest. Indeed, it has been suggested that after binding of the

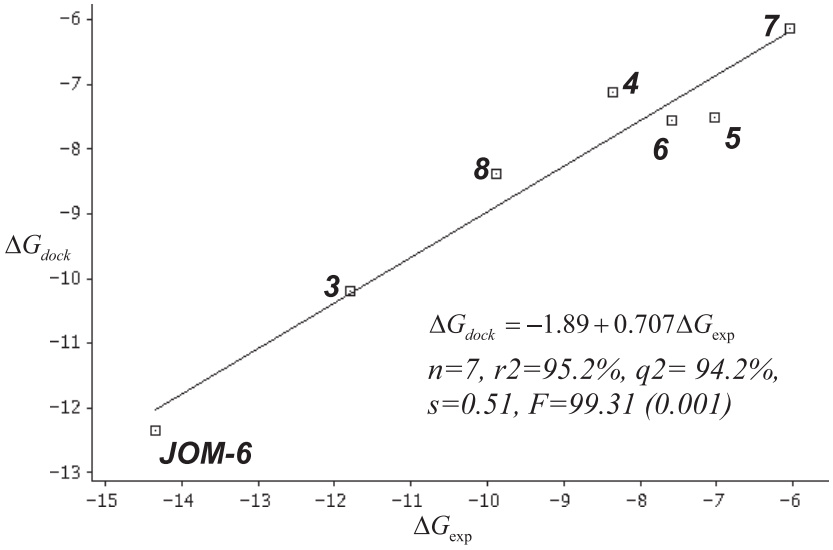

Fig. 14. Correlation between the experimental (ΔG_{exp}) and docking (ΔG_{dock}) free energies calculated in the ligand-binding domain of the MOR model. Relevant statistical parameters are also included.

agonist JOM-6, Trp293 of TMH VI is forced to rotate to form an efficient stacking interaction with Tyr1 of the ligand [51]. The rearrangement of Trp293 would be accompanied by a rigid 20° rotation of TMH VI, leading to the formation of a polar crevice delimited by TMH III, TMH VI, and TMH VII. In particular, this mechanism induces TMH VI to move towards TMH V. The overall helix movement would be responsible for the rearrangement of polar residues in the cytoplasmatic region, so determining the activation of the G protein. Accordingly, the strong stacking interaction of D-Trp3 with Trp293 might be implicated in the modulation of helix motions needed for the activation of the receptor after binding of compound **3**.

Finally, in order to assess the contribution of the QM/MM polarization to the ligand, the interaction energy between compound **3** and the environment was calculated. Despite the small movements of the binding site residues, the QM/MM methods confirm the enhanced binding ability of orientation 2 with respect to orientation 1, measurable by a difference in the binding energy of ~ 21 kcal·mol^{-1} (−9180 and −9201 kcal·mol^{-1} for orientations 1 and 2, respectively), a difference that is almost unpredictable considering only the differences in the binding site composition or in the steric hindrance. When the ligand reaches the binding site, it can be polarized by the asymmetry in charge distribution of the residues with permanent dipole moments (Ser, Thr, Asn, Tyr, Trp, Cys and His) located on the surface of the binding site, and this polarization effect can be obtained by using the QM description of the ligand. Looking at the electronic structure of the ligands in their bounded conformations, we can observe that both orientations tend to support the superimposition of their dipole moments with that of the binding site (Fig. 15).

This conformation is able to promote the binding because the additional dipole moment induced in the ligand results in a stronger Coulomb interaction between compound **3** and the binding site, ensuring a better dipole–dipole interaction with the MOR environment. For both orientation 1 and orientation 2, if the adopted conformations of the ligand are coherent with this scheme, the additional dipole moment contributions caused in the binding site environment give rise to a larger overall dipole moment, with a net contribution to the drug–receptor interaction energy that can vary from −1 to −5 kcal·mol^{-1}. This effect is particularly important for orientation 2, where the better dipole–dipole interaction with the MOR environment results in an overall dipole moment of 133 Debye, as compared to the value obtained for orientation 1 (70 Debye). Then, from the analysis of the results of the QM/MM optimization, it appears that principal effect is again the electronic one. This effect, together with the steric hindrance, can be used to direct the binding to the receptor and to score the relative values of the binding energy.

Conclusions

The recent discovery of the atypical CPP compound **3**, c[YpwFG], which activates MOR even when deprived of a protonable amine, could be of interest for devel-

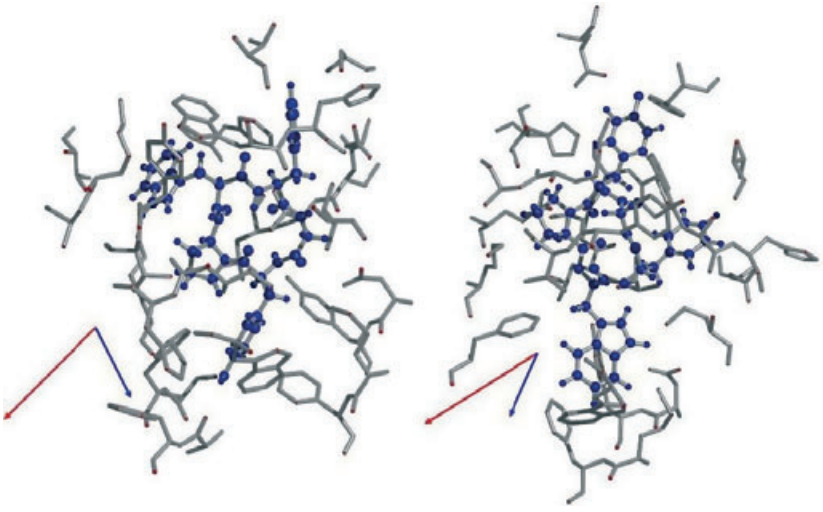

Fig. 15. Representation of the QM part of the MOR–compound **3** complex in orientation 1 (left) and orientation 2 (right). In both cases, the ligand is represented as a ball and stick, and the amino acid portion is shown as a stick. The dipole moments for the binding site (red arrow) and for the ligand (blue arrow) are shown in the bottom left.

oping novel analgesics characterized by alternative ligand–receptor interaction modes. In this work, we have analyzed plausible 3D structures of compound **3** and its analogs compounds **4**–**8**, accounting for the diverse binding affinities towards MORs. The comparison of the structures of the CPPs and JOM-6 suggested that the CPPs probably interact with the receptor by adopting peculiar orientations.

On the basis of spectroscopic analysis, MD, and molecular docking studies, we have restricted the investigation to two orientations of the ligands within the receptor pocket. We first explored the possible binding positions and binding modes of the flexible ligands within the rigid receptor environment, and the solutions obtained from this docking were subsequently optimized by means of the combined QM/MM approach, using a flexible receptor environment that allows simulation of the receptor adaptation upon ligand binding.

The first orientation recalls the traditional models of ligand–receptor complexes reported in the literature (see Discussion). On the other hand, molecular docking analysis furnished a second, plausible, reversed orientation, characterized by a more favorable binding energy after QM/MM geometry optimization, showing the indole NH of D-Trp3 hydrogen bonded to Asp147 of TMH III, plus other interactions with key receptor residues. The absence of the ionic interaction can be partially compendated for by the hydrogen bond of D-Trp3 with Asp147. Also, a highly favorable dipole–dipole interaction was calculated for compound **3** in the orientation 2, indicating that ligand polarization induced by the protein environment represents a noteworthy contribution to the overall binding energy.

This second orientation represents an unusual mode of receptor binding and activation. The good correlation between the observed receptor affinities and the calculated interaction energies for compounds **3**–**8** substantiates the reliability of the model.

In the proposed model, after the initial contact, the reciprocal induced fit [55] of both ligand and receptor would allow the transmission of a deformation from the binding site to the transmembrane domain [51], in particular for the strong interaction between the D-Trp3 aromatic side-chain and Trp293 of TMH VI.

Experimental procedures

General methods

Unless stated otherwise, standard chemicals were obtained from commercial sources (Sigma-Aldrich, St Louis, MO, USA; or Invitrogen, Carlsbad, CA, USA) and used without further purification. Flash chromatography was performed on Merck silica gel 60 (230–400 mesh), and solvents were simply distilled. ESI MS was performed with an HP 1100MSD. Analytical RP-HPLC was performed on an HP Series 1100, with an HP Hypersil ODS column (4.6 μm particle size, 250 mm), diode-array detector 210 nm (eluant: from 90 : 10 to 20 : 80 H_2O/CH_3CN in 15 min, followed by 10 min of 20 : 80 H_2O/CH_3CN). Semipreparative RP-HPLC was performed on an HP Series 1100 using a Zorbax Eclipse XDB C18 column, 7 μm particle size, 21.2 × 150 mm (eluant: 60 : 40 H_2O/CH_3CN for 5 min, then from 60 : 40 H_2O/CH_3CN to 100% CH_3CN in 15 min).

Peptide synthesis [36]

Peptides were prepared by standard solid phase peptide synthesis using Fmoc chemistry. Wang resin (0.5 g, 0.5 $mmol \cdot g^{-1}$) suspended in 9 : 1 dichloromethane/dimethylformamide (5 mL) was treated with a solution of Fmoc-Phe-OH (0.21 g, 0.5 mmol) and HOBt (0.07 g, 0.5 mmol) in dimethylformamide (2 mL), followed by *N*,*N*′-dicyclohexylcarbodiimide (0.11 g, 0.5 mmol) and catalytic dimethylaminopyridine. The mixture was mechanically shaken for 4 h, and then filtered, and the resin was washed with dimethylformamide (5 mL), CH_3OH (5 mL), and dichloromethane (5 mL). To end-cap unreacted OH groups, the resin was suspended in dichloromethane (5 mL), treated with Ac_2O (0.3 mL) and pyridine (0.3 mL), and mechanically shaken. After 0.5 h, the mixture was filtered and the resin was washed twice with dimethylformamide (5 mL), CH_3OH (5 mL), and dichloromethane (5 mL).

The Fmoc group was cleaved from the resin with 4 : 1 dimethylformamide/piperidine (4 mL) under mechanical shaking. After 15 min, the mixture was filtered, and the resin was washed with dichloromethane (5 mL) and treated under mechanical shaking with a second portion of 4 : 1 dimethylformamide/piperidine. After 30 min, the mixture was filtered, and the resin was washed twice with dimethylformamide (5 mL), CH_3OH (5 mL), and dichloromethane (5 mL).

The following residues were introduced by means of the same procedure described above, without catalytic dimethylaminopyridine, and with the exclusion of the end-capping step. Coupling efficacy was determined by means of Kaiser or chloranil tests.

Peptide cleavage

The N-deprotected resin was suspended in a mixture of trifluoroacetic acid (4.7 mL), H_2O (0.15 mL), and PhOH (0.15 mL), and mechanically shaken at room temperature. After 2 h, the mixture was filtered, the resin was washed twice with 10% trifluoroacetic acid in Et_2O (5 mL), and twice with Et_2O, and each filtrate was poured into 100 mL of ice-cold Et_2O. The resulting precipitate was filtered, and

the crude solid peptide–trifluoroacetic acid salt was crystallized from MeOH/Et_2O. Peptides were characterized by analytical RP-HPLC and ESI MS (see General methods).

Peptide cyclization

The peptides (0.1 mmol) were dissolved in dry dimethylformamide (40 mL) and treated while being magnetically stirred with $NaHCO_3$ (4.5 mmol) and DPPA (0.3 mmol) at room temperature. After 2 days, the mixture was filtered, the solvent was distilled at reduced pressure, and the residue was transferred in a separating funnel. The residue was diluted with water (5 mL), and the mixture was extracted with EtOAc (4 × 20 mL). The collected organic layers were dried over Na_2SO_4, and the solvent was evaporated at reduced pressure. The oily residue was purified by flash chromatography over silica gel (eluant: EtOAc/MeOH 97 : 3), followed by semipreparative RP-HPLC (see General methods), affording the cyclopeptides in 50–70% yield, 93–97% pure by analytical RP-HPLC analysis (see General methods). Peptides were characterized by analytical ESI MS (see General methods).

Binding assays

Rat brain, without cerebellum, was weighed and homogenized in 10 volumes of ice-cold 0.32 M sucrose/10 mM Tris/HCl (pH 7.4 at 4 °C). The homogenate was centrifuged at 850 ***g*** for 10 min at 4 °C, and the surnatant was in turn centrifuged at 75 000 ***g*** for 20 min at 4 °C. The resulting pellet was suspended in 10 volumes of 50 mM Tris/HCl/100 mM NaCl (pH 7.4 at 4 °C), as incubation buffer, and incubated for 1 h at 37 °C. to remove any endogenous opioid ligands. After a final centrifugation at 75 000 ***g*** for 20 min at 4 °C, the pellet was stored at −80 °C for up to 2 weeks.

Protein concentration was determined according to Lowry *et al.* [56]. [^{3}H]DAMGO was used as a μ-selective radioligand (1 nM); specific activity was 64 Ci·mmol^{-1}, K_d = 4.85 nM, and B_{max} = 48 fmol·mg^{-1} protein; n = 3. Nonspecific binding was determined in the presence of 100 μM DAMGO. The incubation buffer consisted of 50 mM Tris/HCl, 0.1% BSA (pH 7.4 at 4 °C), and 2 mM EDTA. To prevent any peptidase degradation, the following protease inhibitors were added to the binding buffer: captopril 25 μg·mL^{-1}, bacitracin 0.2 mg·mL^{-1}, leupeptin 10 μg·mL^{-1}, phenylmethylsulfonyl floride 0.19 mg·mL^{-1}, and aprotinin 5 KIU·mL^{-1}. DORs and KORs were blocked with 0.01 M H-Tyr-D-Ala-Gly-Phe-D-Leu-OH and 0.01 M U50 488, respectively.

The mixture (1 mL) was incubated for 1 h at room temperature, and then filtered under vacuum through glass fibers [GFB, Whatman, soaked for 1 h in 0.1% poly(ethyleneimine)] and washed with ice-cold washing buffer (50 mM Tris/HCl, pH 7.4 at 4 °C). The ligand–receptor complex radioactivity retained in the filter was measured by liquid scintillation spectrometry using a scintillator after 12 h of incubation in scintillation cocktail. All assays were performed in triplicate, and repeated at least three times. Stock solutions (10^{-2} M) were in dimethylsulfoxide or MeOH/0.1 M HCl (1 : 1 v/v).

NMR experiments

NMR spectra were recorded using 5 mm tubes, using 0.01 M peptide in dimethylsulfoxide-d_6, at 400 MHz and room temperature. Chemical shifts are reported as δ values relative to the solvent peak. VT-^{1}H-NMR experiments were performed over the range 298–348 K. 2D spectra were acquired in the phase-sensitive mode and processed using a 90° shifted, squared sine-bell apodization. The unambiguous assignment of the resonances was performed by Gradient COSY and heteronuclear multiple bond correlation (HBMC) analysis. GradientCOSY experiments were recorded with a proton spectral width of 9595.8 Hz. Gradient HMBC experiments were recorded with a proton spectral width of 9595.8 Hz and a carbon spectral width of 36 199.1 Hz, selecting a spin coupling constant of 8 Hz. ROESY experiments were recorded with a 300 ms mixing time with a proton spectral width of 3087.8 Hz.

Conformational analysis in solution

The data derived from 2D-ROESY in dimethylsulfoxide-d_6 were analyzed by restrained MD, using nongeminal interproton distances as constraints. When possible, an analysis of $^3J_{NH–H\alpha}$ and $^3J_{H\alpha–H\beta}$ coupling constants was used to estimate the torsion angles [57]. The eventual presence of $H\alpha_i$–$H\alpha_{i+1}$ cross-peaks was used to infer the presence of *cis* peptide bonds. Also, the difference between the ^{13}C-NMR chemical shifts (data not shown) of Pro-Cβ and Pro-Cγ (e.g. at 26.7 and 24.3, respectively, for D-Pro2 in compound **3**) confirmed the configuration of the preceding peptide bond (a $\Delta\delta$ Cβ–Cγ of 4–6 p.p.m. indicates a *trans* peptide bond, whereas a $\Delta\delta$ Cβ–Cγ of 8–10 p.p.m. is expected for a *cis* one) [58]. The gas-phase MD simulations were conducted at 298 K by using an AMBER [39] force field with a distance dependent ε = 4.0 r. In the restrained MD, a 50 ps simulation at 1200 K was used for generating 100 random structures that were subsequently subjected to a 20 ps restrained MD simulation with a 50% scaled force field at the same temperature, followed by 20 ps at 1200 K with full restraints, after which the system was cooled in 10 ps to 50 K. The distance force constant was 7 kcal·mol^{-1}·Å^{-2}; ω-bonds were set at 180°, using a force constant of 16 kcal·mol^{-1}·Å^{-2}. Only ROESY-derived constraints were included in the restrained MD. ROESY intensities were classified according to a calibration against the intensity of geminal protons. Very strong, strong, medium and weak signals were associated with distances of < 2.3, < 2.8,

< 3.5 and < 4.8 Å, respectively. Geminal couplings ad other obvious correlations were discarded.

The resulting structures were minimized with 3000 cycles of steepest descent and 3000 cycles of conjugated gradient; convergence was at 0.01 kcal·Å^{-1}·mol^{-1}. The structures that showed the lowest internal energy and the least number of violations of the experimental data were selected and analyzed.

Simulations in explicit water were performed at 298 K, again using the AMBER force field in a $30 \times 30 \times 30$ box of standard TIP3P models of equilibrated water [59,60], with a minimum solvent–solute distance of 2.3 Å, at constant temperature and pressure (Berendsen scheme [61], bath relaxation constant 0.2).

Computational procedures

Molecular modeling and graphics manipulations were performed using optimized Mac OSX versions of NAMD [62], AUTODOCK [30], AUTODOCK TOOLS [63] and UCSF CHIMERA software packages [64] on an Apple® MacPro quad-Xeon workstation running Mac OSX Tiger (version 10.4.9). Model building and geometry optimizations of the studied compounds were accomplished with the GAUSSIAN 03 (6-31G* base set) [43] quantum mechanical calculations package. The outputs from AUTODOCK and all modeling studies as well as images were built with PYMOL [42] and ACCELRYS DSVISUALIZER (http://www.accelrys.com) and rendered with POVRAY [65]. UCSF CHIMERA was used to calculate the hydrogen bond distances measured between the hydrogen and its assumed binding partner. The MOR–substrate complex was constructed by docking the ligand into the equilibrated MOR structure using AUTODOCK. Then, the system was equilibrated with a series of minimizations interspersed by short MD simulations; the resulting structures were used as the starting model for the GAUSSIAN 03 QM/MM study, as well as for a 1.2 ns MD simulation, and the structure resulting from MD simulation was then optimized by means of an AMBER force field.

Preparation of the MOR–substrate systems

As the experimentally determined 3D structure of a MOR is not yet available, a MOR 3D model was generated using MODELLER according to the protocol of comparative modeling [66]. The sequence of the MOR polypeptide chain was retrieved from the Swiss-Prot database and aligned using the PAM250 matrix, using 'gap-open' and 'gap-elongation' penalties of 10 and 0.05, respectively. The alignment was then manually refined to ensure a perfect alignment of the highly conserved residues. The homology model of the MOR receptor was built by introducing into the MODELLER program [66] the X-ray rhodopsin crystal structure (Protein Data Bank code: 1f88), selected as the template structure from the Protein Data Bank using a GAPPED BLAST OF PROTEIN SIMILARITY SEARCH module. The MOR model was then checked through AUTODOCK TOOLS and UCSF CHIMERA to guarantee system conformity with the molecular modeling programs (in particular, the names of the side chains that must be congruent with the AMBER force field used). The amino acid chain of the MOR model was terminated with $-COO^-$ and $-NH_3^+$ groups in their zwitterionic forms, and the polar hydrogen atoms were added in their calculated positions. The protonation state was set to the normal ionization state at pH 7.0 for all the ionizable residues (in particular, Asp147, Asp216, Glu229 and Glu310) and His residues (His223, His297 and His319 set to Nδ1), and both the topology and connectivity of the molecule had been created. Model building was followed by energy minimization up to an energy gradient lower than 10^{-4} kcal·mol^{-1}·Å^{-1}, choosing AMBER as a force field as implemented in the NAMD package. Thus, the model was compared with the agonist peptide-incorporated structural model of MOR constructed by Mosberg *et al.* [50] (model title: OPRM_RAT_AD_JOM-6, available from the Mosberg Lab studies on peptide synthesis and molecular recognition at the University of Michigan in Ann Arbor [67]), and no inconsistencies were observed (rmsd value of 0.20 Å).

The experimental conformations preferentially adopted in dimethylsulfoxide solution were used as starting structures, whereas that of JOM-6 was obtained from the original Mosberg MOR model. The ligands were then optimized using GAUSSIAN 03 at the B3LYP/6-31G* level [43,68], and atomic charges were assigned using the Gasteiger–Marsili formation, which uses the type of atomic charges used in calibrating the AUTODOCK empirical free energy function [69].

Molecular docking

To test the ability of the molecular docking program to reveal the ligand binding to our MOR, the JOM-6 molecule was initially docked, and the orientation of the resulting lowest-energy structure was compared with that present in the original Mosberg model [50,51]. A perfect superposition (rmsd 0.33 Å) was obtained, a result that demonstrates the ability of AUTODOCK to locate the JOM-6 binding mode. The docking into the MOR model was performed with AUTODOCK (version 4) [30,64]. The AUTODOCK suite uses an automated docking approach that allows ligand flexibility, and it is able to locate docking poses in a consistent way with respect to the X-ray crystal structures [32,70]. Default parameters (including a distance-dependent dielectric 'constant') were used as described in the AUTODOCK manual, and both the protein crystal structure and the ligands were prepared for docking by following the default protocols (except for those changes mentioned below). AUTODOCK uses an empirical

scoring function that is able to approximate the binding free energies, because it includes a solvation free energy term. Because of the absence of information on the binding region for compounds **3**, **7**, and **8**, the docking process was performed in two steps. In the first, the docking procedure was applied to the whole protein target, without imposing any binding site, using the so-called 'blind docking' approach [31,71]. A box of $40 \times 40 \times 40$ Å, centered at the middle of the MOR model, was used with a grid resolution of 0.5 Å. The resulting docked conformations were clustered into families of similar binding modes, with an rmsd clustering tolerance of 2 Å. In almost all cases, the lowest docking energy conformations were included in the largest cluster found (which usually contains 80–100% of total conformations). Otherwise, the lowest docking energy conformations were considered to be the most stable orientations. In the second step, we docked the ligands in the binding site found in the first step ('refined docking'). This time, a box of $20 \times 20 \times 20$ Å, centered on the best scored conformation obtained in the first step (corresponding to *x*-, *y*- and *z*-values of −13.71, 9.56 and 0.47 Å, respectively), was considered, with a grid resolution of 0.300 Å. Movement of the ligands was limited to inside this search space during docking. Atomic solvation parameters were assigned to the protein, and the default parameters for the Lamarckian genetic algorithm were used as the search protocol, except for the maximum number of energy evaluations, which was changed to 10 million (the population size was raised to 500). For the GA algorithm, the default parameters were kept for mutation, crossover, and elitism. The docked energy also includes the ligand internal energy or the intramolecular interaction energy of the ligand. AUTODOCK also reports a binding free energy that excludes the ligand internal energy but includes a torsional free energy term for the ligand based on the number of rotatable bonds. The resulting orientations were again clustered into families, considering a rmsd clustering tolerance of 2.0 Å, and the lowest docking energy conformations were equilibrated for 1.2 ns by unrestrained MD, choosing AMBER as a force field as implemented in the NAMD package. The simulations were performed at constant temperature and pressure (NPT ensemble) in a periodic cubic box of TIP3P water molecules. The bond distances and bond angles of water were constrained using the SETTLE algorithm [72], and the bond lengths within the protein were constrained with the LINCS algorithm [73]. The coupling time was set to 1.0 ps, and the isothermal compressibility was set to 4.6×10^{-5}·bar^{-1}. The protein, ligand and solvent were independently coupled to a temperature of 298 K with a coupling time of 0.1 ps, and the pressure was held at 1 bar, with a coupling time of 0.2 ps, using a Berendsen thermostat to maintain the constant temperature and pressure. The time step used was 1.0 fs. Snapshots of the MOR–substrate systems were saved every 0.2 ps, and 6000 snapshots were saved. Hydrogen bonds and contacts were automatically identified using the 'contact' module of CCP4 [74] and UCSF CHIMERA, and the other interactions were identified visually.

Hybrid QM/MM calculations

In the current study, we used the pseudo-bond *ab initio* QM/MM approach as implemented in GAUSSIAN 03 [43,68]. This methodology circumvents the major deficiency of the conventional link-atom QM/MM approach by providing a consistent and well-defined *ab initio* QM/MM potential-energy surface. For the QM/MM calculations, the MOR–ligand system resulting from the docking study was first partitioned into a QM subsystem and an MM subsystem. The reaction system used a smaller QM subsystem consisting of the cyclopeptide and side chains of the amino acids within 3.5 Å from orientations 1 and 2, whereas the rest of the protein (the MM subsystem) was treated using the AMBER force field, together with a low memory convergence algorithm. The boundary problem between the QM and MM subsystems was treated using the pseudo-bond approach. With this MOR–substrate QM/MM system, an iterative optimization procedure was applied to the QM/MM system, using B3LYP/3-21G* QM/MM calculations, leading to an optimized structure for the reactants. The convergence criterion used was set to obtain an energy gradient of $< 10^{-4}$, using the twin-range cutoff method for nonbonded interactions, with a long-range cutoff of 14 Å and a short-range cutoff of 8 Å.

Acknowledgements

We thank Fondazione CARISBO, Bologna, MIUR (PRIN 2004), Bologna University (Funds for Selected Topics) for providing financial support, and Indena S.p.A. for a grant to R. Artali.

References

1 Burden JE, Davis P, Porreca F & Spatola AF (1999) Synthesis and biological activities of position one and three transposed analogs of the opioid peptide YKFA. *Bioorg Med Chem Lett* **9**, 3441–3446.

2 Mosberg HI, Ho JC & Sobczyk-Kojiro K (1998) A high affinity, mu-opioid receptor-selective enkephalin analogue lacking an N-terminal tyrosine. *Bioorg Med Chem Lett* **8**, 2681–2684.

3 McFadyen IJ, Sobczyk-Kojiro K, Schaefer MJ, Ho JC, Omnaas JR, Mosberg HI & Traynor JR (2000) Tetrapeptide derivatives of [D-Pen2,D-Pen5]-enkephalin (DPDPE) lacking an N-terminal tyrosine residue are agonists at the μ-opioid receptor. *J Pharmacol Exp Ther* **295**, 960–966.

4 Zdzislaw SA & Schiller PW (2000) Optically active aromatic amino acids. Part VI. Synthesis and properties of [Leu5]-enkephalin analogues containing *O*-methyl-L-tyrosine1 with ring substitution at position 3′. *J Pept Sci* **6**, 280–289.
5 Ambo A, Terashima T & Sasaki Y (2002) Novel [D-Arg2]dermorphin(1–4) analogs with mu-opioid receptor antagonist activity. *Chem Pharm Bull* **50**, 1401–1403.
6 Dolle RE, Machaut M, Martinez-Teipel B, Belanger S, Cassel JA, Stabley GJ, Graczykb TM & DeHaven RN (2004) (4-Carboxamido)phenylalanine is a surrogate for tyrosine in opioid receptor peptide ligands. *Bioorg Med Chem Lett* **14**, 3545–3548.
7 Schiller PW, Berezowska I, Nguyen TM-D, Schmidt R, Lemieux C, Chung NN, Falcone-Hindley ML, Yao W, Liu J, Iwama S *et al.* (2000) Novel ligands lacking a positive charge for the δ- and μ-opioid receptors. *J Med Chem* **43**, 551–559.
8 Cardillo G, Gentilucci L, Tolomelli A, Qasem AR, Spampinato S & Calienni M (2003) Conformational analysis and μ-opioid receptor affinity of short peptides, endomorphin models in a low polarity solvent. *Org Biomol Chem* **1**, 3010–3014.
9 Lu Y, Weltrowska G, Lemieux C, Chung NN & Schiller PW (2001) Stereospecific synthesis of (2*S*)-2-methyl-3-(2′,6′-dimethyl-4′-hydroxyphenyl)-propionic acid (Mdp) and its incorporation into an opioid peptide. *Bioorg Med Chem Lett* **11**, 323–325.
10 Lu Y, Nguyen TM, Weltrowska G, Berezowska I, Lemieux C, Chung NN & Schiller PW (2001) 2′,6′-Dimethyltyrosine]dynorphin A(1–11)-NH2 analogues lacking an N-terminal amino group: potent and selective κ-opioid antagonists. *J Med Chem* **44**, 3048–3053.
11 Vig BS, Murray TF & Aldrich JV (2003) A novel N-terminal cyclic dynorphin A analogue *cycloN,5*[Trp3,Trp4,Glu5] dynorphin A-(1–11)NH2 that lacks the basic N-terminus. *J Med Chem* **46**, 1279–1282.
12 Eguchi M, Shen RY, Shea JP, Lee MS & Kahn M (2002) Design, synthesis, and evaluation of opioid analogues with non-peptidic β-turn scaffold: enkephalin and endomorphin mimetics. *J Med Chem* **45**, 1395–1398.
13 Yan F & Roth BL (2004) Salvinorin A: a novel and highly selective κ-opioid receptor agonist. *Life Sci* **75**, 2615–2619.
14 Roth BL, Baner K, Westkaemper R, Siebert D, Rice KC, Steinberg S, Ernsberger P & Rothman RB (2002) Salvinorin A: a potent naturally occurring nonnitrogenous κ-opioid selective agonist. *Proc Natl Acad Sci USA* **99**, 11934–11939.
15 Munro TA, Rizzacasa MA, Roth BL, Toth BA & Yan F (2005) Studies toward the pharmacophore of salvinorin A, a potent κ-opioid receptor agonist. *J Med Chem* **48**, 345–348.
16 Yan F, Mosier PD, Westkaemper RB, Stewart J, Zjawiony JK, Vortherms TA, Sheffler DJ & Roth BL (2005) Identification of the molecular mechanisms by which the diterpenoid salvinorin A binds to j-opioid receptors. *Biochemistry* **44**, 8643–8651.
17 Beguin C, Richards MR, Wang Y, Chen T, Liu-Chen LY, Ma Z, Lee DYW, Carlezon WA Jr & Cohen BM (2005) Synthesis and in vitro pharmacological evaluation of salvinorin A analogues modified at C(2). *Bioorg Med Chem Lett* **15**, 2761–2765.
18 Harding WW, Tidgewell K, Byrd N, Cobb H, Dersch CM, Butelman ER, Rothman RB & Prisinzano TE (2005) Neoclerodane diterpenes as a novel scaffold for μ-opioid receptor ligands. *J Med Chem* **48**, 4765–4771.
19 Kane BE, Nieto MJ, McCurdy CR & Ferguson DM (2006) A unique binding epitope for salvinorin A, a non-nitrogenous kappa opioid receptor agonist. *FEBS J* **273**, 1966–1974.
20 Cardillo G, Gentilucci L, Tolomelli A, Spinosa R, Calienni M, Qasem AR & Spampinato S (2004) Synthesis and evaluation of the affinity toward μ-opioid receptors of atypical, lipophilic ligands based on the sequence *c*[-Tyr-Pro-Trp-Phe-Gly-]. *J Med Chem* **47**, 5198–5203.
21 Kessler H (1982) Conformation and biological activity of cyclic peptide. *Angew Chem Int Ed Engl* **21**, 512–523.
22 Kessler H, Gratias R, Hessler G, Gurrath M & Mueller G (1996) Conformation of cyclic peptides. Principle concepts and the design of selectivity and superactivity in bioactive sequences by spatial screening. *Pure Appl Chem* **68**, 1201–1205.
23 Dechantsreiter MA, Planker E, Matha B, Lohof E, Holzemann G, Jonczyk A, Goodman SL & Kessler H (1999) *N*-Methylated cyclic RGD peptides as highly active and selective αVβ3 integrin antagonists. *J Med Chem* **42**, 3033–3040.
24 Tamamura H, Mizumoto M, Hiramatsu K, Kusano S, Terakubo S, Yamamoto N, Trent J-O, Wang Z, Peiper SC, Nakashima H *et al.* (2004) Topochemical exploration of potent compounds using retro-enantiomer libraries of cyclic pentapeptides. *Org Biomol Chem* **2**, 1255–1257.
25 Weisshoff H, Prasang C, Henklein P, Frommel C, Zschunke A & Mugge C (1999) Mimicry of βII′-turns of proteins in cyclic pentapeptides with one and without D-amino acids. *Eur J Biochem* **259**, 776–788.
26 Stradley SJ, Rizo J, Bruch MD, Stroup AN & Gierasch LM (1990) Cyclic pentapeptides as models for reverse turns: determination of the equilibrium distribution between type I and type II conformations of Pro-Asn and Pro-Ala β-turns. *Biopolymers* **29**, 263–287.
27 Wermuth J, Goodman L, Jonczyk A & Kessler H (1997) Stereoisomerism and biological activity of the

selective and superactive αvβ3 integrin inhibitor cyclo(RGDfV) and its retro-inverso peptide. *J Am Chem Soc* **119**, 1328–1335.
28 Gentilucci L & Tolomelli A (2004) Recent advances in the investigation of the bioactive conformation of peptides active at the μ-opioid receptor. Conformational analysis of endomorphins. *Curr Topics Med Chem* **4**, 105–121.
29 Leitgeb B, Szekeres A & Toth G (2003) Conformational analysis of endomorphin-1 by molecular dynamics methods. *J Pept Res* **62**, 145–157.
30 Morris GM, Goodsell DS, Halliday RS, Huey R, Hart WE, Belew RK & Olson AJ (1998) Automated docking using a Lamarckian genetic algorithm and empirical binding free energy function. *J Comp Chem* **19**, 1639–1662.
31 Hetényi C & van der Spoel D (2002) Efficient docking of peptides to proteins without prior knowledge of the binding site. *Protein Sci* **11**, 1729–1737.
32 Hetényi C & van der Spoel D (2006) Blind docking of drug-sized compounds to proteins with up to a thousand residues. *FEBS Lett* **580**, 1447–1450.
33 Gao J (1992) Methods and applications of combined quantum mechanical and molecular mechanical potentials. In *Reviews in Computational Chemistry*, **Vol. 7** (Lipkowitz KB & Boyd DB, eds), pp. 119–185. VCH, New York, NY.
34 Zhang Y, Lee T & Yang W (1999) A pseudobond approach to combining quantum mechanical and molecular mechanical methods. *J Chem Phys* **110**, 46–54.
35 Schweitzer-Stenner R, Gonzales W, Bourne GT, Feng JA & Marshall GR (2007) Conformational manifold of r-aminoisobutyric acid (Aib) containing alanine-based tripeptides in aqueous solution explored by vibrational spectroscopy, electronic circular dichroism spectroscopy, and molecular dynamics simulations. *J Am Chem Soc* **129**, 13095–13109.
36 Kates SA & Albericio F, Eds (2001) *Solid-Phase Synthesis*. pp. 1–826. Dekker, New York, NY.
37 Temussi PA, Picone D, Saviano G, Amodeo P, Motta A, Tancredi T, Salvadori S & Tomatis R (1992) Conformational analysis of an opioid peptide in solvent media that mimic cytoplasm viscosity. *Biopolymers* **32**, 367–372.
38 Toniolo C (1980) Intramolecularly hydrogen-bonded peptide conformations. *CRC Crit Rev Biochem* **9**, 1–44.
39 Cornell WD, Cieplak P, Bayly CI, Gould IR, Merz KM, Ferguson DM, Spellmeyer DC, Fox T, Caldwell JW & Kollman PA (1995) A second-generation force field for the simulation of proteins, nucleic acids, and organic molecules. *J Am Chem Soc* **117**, 5179–5197.
40 Steglich W & Paulitz C (1997) Stereoselective modification of a cyclopentapeptide via an α-(ethylthio)glycine residue. *J Org Chem* **62**, 8474–8478.
41 Eguchi M (2004) Recent advances in selective opioid receptor agonists and antagonists. *Med Res Rev* **24**, 182–212.
42 DeLano WL (2002) *PyMol Molecular Graphics System*. DeLano Scientific, San Carlos, CA.
43 Frisch MJ, Trucks GW, Schlegel HB, Scuseria GE, Robb MA, Cheeseman JR, Montgomery JA, Vreven T, Kudin KN, Burant JC *et al*. (2003) *Gaussian 03*. Revision A.1. Gaussian, Pittsburgh, PA.
44 Podlogar BL, Paterlini MG, Ferguson DM, Leo GC, Demeter DA, Brown FK & Reitz AB (1998) Conformational analysis of the endogenous mu-opioid agonist endomorphin-1 using NMR spectroscopy and molecular modeling. *FEBS Lett* **439**, 13–20.
45 Janecka A, Fichna J, Mirowski M & Janecki T (2002) Structure–activity relationship, conformation and pharmacology studies of morphiceptin analogues – selective mu-opioid receptor ligands. *Mini Rev Med Chem* **2**, 565–572.
46 Malicka J, Czaplewski C, Groth M, Wiczk W, Oldziej S, Lankiewicz L, Ciarkowski J & Liwo A (2004) Use of NMR and fluorescence spectroscopy as well as theoretical conformational analysis in conformation–activity studies of cyclic enkephalin analogues. *Curr Topics Med Chem* **4**, 123–133.
47 Paterlini MG, Avitabile F, Ostrowski BG, Ferguson DM & Portoghese PS (2000) Stereochemical requirements for receptor recognition of the mu-opioid peptide endomorphin-1. *Biophys J* **78**, 590–599.
48 Grieco P, Giusti L, Carotenuto A, Campiglia P, Calderon V, Lama T, Gomez-Monterrey I, Tartaro G, Mazzoni MR & Novellino E (2005) Morphiceptin analogues containing a dipeptide mimetic structure: an investigation on the bioactive topology at the μ-receptor. *J Med Chem* **48**, 3153–3163.
49 Hruby VJ & Agnes RS (1999) Conformation–activity relationships of opioid peptides with selective activities at opioid receptors. *Biopolymers* **51**, 391–410.
50 Mosberg HI & Fowler CB (2002) Development and validation of opioid ligand–receptor interaction models: the structural basis of mu vs. delta selectivity. *J Pept Res* **60**, 329–335.
51 Fowler CB, Pogozheva ID, Lomize AL, LeVine H & Mosberg HI (2004) Complex of an active μ-opioid receptor with a cyclic peptide agonist modeled from experimental constraints. *Biochemistry* **43**, 15796–15810.
52 Hruby VJ & Gehrig CA (1989) Recent developments in the design of receptor specific opioid peptides. *Med Res Rev* **9**, 343–401.
53 Tomboly C, Kover KE, Peter A, Tourwe D, Biyashev D, Benyhe S, Borsodi A, Al-Khrasani M, Ronai AZ & Toth G (2004) Structure–activity study on the Phe side chain arrangement of endomorphins using conformationally constrained analogues. *J Med Chem* **47**, 735–743.

54 In Y, Minora K, Tomoo K, Sasaki Y, Lazarus LH, Okada Y & Ispida T (2005) Structural function of C-terminal amidation of endomorphin. *FEBS J* **272**, 5079–5097.
55 Davis AM & Teague SJ (1999) Hydrogen bonding, hydrophobic interactions, and failure of the rigid receptor hypothesis. *Angew Chem Int Ed Engl* **38**, 736–749.
56 Lowry OH, Rosenbrough NJ, Farr AL & Randall RJ (1951) Protein measurement with the Folin phenol reagent. *J Biol Chem* **193**, 265–275.
57 Cung MT & Marraud M (1982) Conformational dependence of the vicinal proton coupling constant for the Cα–Cβ bond in peptides. *Biopolymers* **21**, 953–967.
58 Konat RK, Mierke DF, Kessler H, Kutscher B, Bernd M & Voegeli R (1993) Synthesis and solvent effects on the conformation of hymenistatin 1. *Helv Chim Acta* **76**, 1649–1666.
59 Berendsen HJC, Postma JPM, van Gunsteren WF, Hermans J & Pullman B (1981) *Intermolecular Forces*. Reidel, Dordrecht.
60 Jorgensen WL, Chandrasekhar J, Madura J, Impey RW & Klein ML (1983) Comparison of simple potential functions for simulating liquid water. *J Chem Phys* **79**, 926–933.
61 Berendsen HJC, Postma JPM, van Gunsteren WF, DiNola A & Haak JR (1984) Molecular dynamics with coupling to an external bath. *J Chem Phys* **81**, 3684–3690.
62 Phillips JC, Braun R, Wang W, Gumbart J, Tajkhorshid E, Villa E, Chipot C, Skeel RD, Kale L & Schulten K (2005) Scalable molecular dynamics with NAMD. *J Comp Chem* **26**, 1781–1802.
63 Sanner MF (1999) Python: a programming language for software integration and development. *J Mol Graphics Mod* **17**, 57–61.
64 Pettersen EF, Goddard TD, Huang CC, Couch GS, Greenblatt DM, Meng EC & Ferrin TE (2004) UCSF Chimera – a visualization system for exploratory research and analysis. *J Comp Chem* **25**, 1605–1612.
65 Persistence of Vision Pty. Ltd (2004) *Persistence of Vision Raytracer (Version 3.6)*. Available at: http://www.povray.org/download/.
66 Fiser A & Sali A (2003) Modeller: generation and refinement of homology-based protein structure models. *Methods Enzymol* **374**, 461–491.
67 The Mosberg Lab University of Michigan in Ann Arbor (2008). Available at: http://mosberg-lab.phar.umich.edu.
68 Hehre W, Radom L, Schleyer P & Pople J (1986) *Ab Initio Molecular Orbital Theory*. John Wiley, New York, NY.
69 Huey R, Morris GM, Olson AJ & Goodsell DS (2007) A semiempirical free energy force field with charge-based desolvation. *J Comp Chem* **28**, 1145–1152.
70 Dym O, Xenarios I, Ke H & Colicelli J (2002) Molecular docking of competitive phosphodiesterase inhibitors. *Mol Pharmacol* **61**, 20–25.
71 Rao MS & Olson AJ (1999) Modelling of factor Xa–inhibitor complexes: a computational flexible docking approach. *Proteins* **34**, 173–183.
72 Miyamoto S & Kollman PA (1992) SETTLE – an analytical version of the shake and rattle algorithm for rigid water models. *J Comput Chem* **13**, 952–962.
73 Hess B, Bekker H, Berendsen HJC & Fraaije JGEM (1997) LINCS: a linear constraint solver for molecular simulations. *J Comput Chem* **18**, 1463–1472.
74 Collaborative Computational Project, Number 4 (1994) The CCP4 Suite: programs for protein crystallography. *Acta Crystallogr* **D50**, 760–763.

Supplementary material

The following supplementary material is available online:

Doc. S1. Spectroscopic characterization of compounds **3**, **7** and **8**.

Fig. S1. ^{1}H-NMR spectra of compounds **3**, **7** and **8**.

Figs S2–S4. ROESY analyses of compounds **3**, **7** and **8**, respectively.

Fig. S5. Side and top views of compounds **3–8** in orientation 1 and orientation 2 docked into the binding site of MOR.

Table S1. $\Delta\delta/\Delta t$ values of amide protons for compounds **3**, **7** and **8**.

Tables S2–S4. ROESY cross-peaks for compounds **3**, **7** and **8**, respectively.

Table S5. Characterization of receptor binding pocket in the two orientations of compound **3** identified by AUTODOCK.

Tables S6–S11. QM/MM characterization of receptor binding pocket in the two orientations of compounds **3–8**, respectively.

This material is available as part of the online article from http://www.blackwell-synergy.com

Please note: Blackwell Publishing are not responsible for the content or functionality of any supplementary materials supplied by the authors. Any queries (other than missing material) should be directed to the corresponding author for the article.